Biophysical Journal
Article

Biophysical Society

Taking Simultaneous Snapshots of Intrinsically Disordered Proteins in Action

Marco Schiavina,[1] Maria Grazia Murrali,[1] Letizia Pontoriero,[1] Valerio Sainati,[1] Rainer Kümmerle,[2] Wolfgang Bermel,[3] Roberta Pierattelli,[1,*] and Isabella C. Felli[1,*]
[1]Magnetic Resonance Center and Department of Chemistry "Ugo Schiff," University of Florence, Sesto Fiorentino, Florence, Italy; [2]Bruker BioSpin AG, Fällanden, Switzerland; and [3]Bruker BioSpin GmbH, Rheinstetten, Germany

ABSTRACT Intrinsically disordered proteins (IDPs) as well as intrinsically disordered regions (IDRs) of complex protein machineries have recently been recognized as key players in many cellular functions. NMR represents a unique tool to access atomic resolution structural and dynamic information on highly flexible IDPs/IDRs. Improvements in instrumental sensitivity made heteronuclear direct detection possible for biomolecular NMR applications. The CON experiment has become one of the most useful NMR experiments to get a snapshot of an IDP/IDR in conditions approaching physiological ones. The availability of NMR spectrometers equipped with multiple receivers now enables the acquisition of several experiments simultaneously instead of one after the other. Here, we propose several variants of the CON experiment in which, during the recovery delay, a second two-dimensional experiment is acquired, either based on ^{1}H detection (CON//HN) or on ^{15}N detection (CON//btNH, CON//(H)CAN). The possibility to collect simultaneous snapshots of an IDP/IDR through different two-dimensional spectra provides a novel tool to follow chemical reactions, such as the occurrence of posttranslational modifications, as well as to study samples of limited lifetime such as cell lysates or whole cells.

SIGNIFICANCE The exploitation of multiple receivers available in most of the newly designed NMR spectrometers enables the simultaneous collection of several snapshots of the very same event from different atomic perspectives.

INTRODUCTION

Proteins or protein regions that lack a well-defined three-dimensional (3D) structure and that are characterized by high flexibility and disorder are widespread in living organisms and essential for protein function (1–3). Their contributions to biological processes are highly complementary to those typical of folded proteins. Indeed, intrinsically disordered proteins (IDPs) or intrinsically disordered protein regions (IDRs) are often involved in key regulatory processes for which the adaptability of the protein structure and dynamics represents a clear functional advantage (4). Their important functional role also becomes evident from the strong link that has been found between misfunction in IDPs/IDRs and many diseases such as cancer and neurodegenerative diseases. The atomic-level characterization of IDPs/IDRs has thus become a topic of central importance also in light of the development of new drugs capable of interfering with them, a completely novel area for which the traditional approach of drug design based on the identification of well-defined binding pockets in folded proteins is obviously bound to fail (5–8).

NMR plays a central role in this area of research being the only method able to provide atomic resolution information on the structural and dynamic properties of highly flexible macromolecules (9–13). NMR observables are, however, strongly influenced by the peculiar properties of IDPs, and thus the NMR approaches should be optimized to overcome critical points (14). For example, it is well known that ^{1}H-detected experiments, usually the first choice on the grounds of instrumental sensitivity, do have some drawbacks for the study of IDPs, in particular when approaching physiological pH and temperature conditions. In fact, the largely solvent-exposed backbones typical of highly flexible IDPs leave amide protons accessible to the solvent and are responsible for efficient chemical exchange processes that may lead to extreme broadening of H^{N} resonances, reducing the sensitivity of ^{1}H-detected experiments. In addition, ^{1}H nuclear

Submitted March 29, 2019, and accepted for publication May 14, 2019.
*Correspondence: roberta.pierattelli@unifi.it or felli@cerm.unifi.it
Editor: David Eliezer.
https://doi.org/10.1016/j.bpj.2019.05.017

spins are characterized by a moderate chemical shift dispersion. These are two features that have stimulated the development of exclusively heteronuclear NMR experiments based on ^{13}C direct detection for the study of IDPs. The two-dimensional (2D) CON experiment (15,16) is now widely used to characterize highly flexible IDPs, thanks to the excellent chemical shift dispersion of the crosspeaks observed in this experiment and the possibility to reveal atomic resolution information on IDPs also in experimental conditions in which H^N resonances are not observable (17–28). The wide use of exclusively heteronuclear NMR experiments for protein investigations has been stimulated by improvements in instrumental sensitivity (29). Technological advances provided a jump of a factor of more than 10 in ^{13}C instrumental sensitivity, and lately, similar efforts have even enabled direct detection of ^{15}N (30–33), a nucleus characterized by a lower gyromagnetic ratio with respect to ^{13}C and thus by a very low intrinsic sensitivity.

In parallel to significant increase in instrumental sensitivity, new technologies have also become easily accessible such as the possibility to exploit NMR spectrometers with multiple receivers, enabling the design of multinuclear pulse sequences for the acquisition of more than one free induction decay (FID) for each repetition. Several different strategies exploiting multiple receivers have been proposed in the literature (34–39) to acquire more experiments in the time needed for a single one. Applications of multiple receivers for biomolecular NMR experiments were also proposed either in solution or in the solid state (36–41). One strategy consists of the acquisition of different FIDs within one main coherence transfer pathway to recover signals that would otherwise be lost or suppressed (36,37). The other strategy consists in exploiting polarization that remains unused at the end of one experiment to collect more than one spectrum in the time needed for the longest one of them (38).

The development of more sensitive instruments and the possibility to use multiple receivers stimulates the design of novel experimental strategies to investigate IDPs, and we will show some examples of the useful information that can be gathered combining the CON with other experimental schemes.

MATERIALS AND METHODS

Samples preparation

The ^{13}C, ^{15}N-labeled α-synuclein sample was prepared as previously described in the literature (42), with a final concentration of 1.0 mM in 100 mM NaCl, 50 μM ethylenediaminetetraacetic acid (EDTA), and 20 mM phosphate buffer at different pH between 6.5 and 7.4 with the addition of 2–10% D_2O for the lock. Each figure reports the details about sample conditions. The ^{13}C, ^{15}N-labeled α-synuclein samples used for in-cell experiments and for experiments on cell lysate were prepared as previously described (43) with an estimated protein concentration of 250 μM, using the same buffer as for the purified samples at pH 7.4.

For the phosphorylation reaction, 700 U of tyrosine kinase Fyn (Sigma Aldrich, St. Louis, MO) were added to a 200 μM sample of ^{13}C, ^{15}N-labeled α-synuclein in 20 mM phosphate buffer, 100 mM NaCl, 50 μM EDTA, 2 mM dithiothreitol, 6 mM $MgCl_2$, and 3 mM ATP buffer at pH 7.0 for a final volume of 300 μL, with 5% D_2O added for the lock.

NMR experiments

The NMR experiments were acquired at different temperatures on a Bruker AVANCE NEO spectrometer (Billerica, MA) operating at 700.06 MHz ^1H, 176.05 MHz ^{13}C, and 70.97 MHz ^{15}N frequencies equipped with a cryogenically cooled probehead optimized for ^{13}C-direct detection (TXO). Standard radio frequency pulses and carrier frequencies for triple resonance experiments were used and are summarized hereafter. Q5- and Q3-shaped pulses (44) of durations of 300 and 231 μs, respectively, were used for ^{13}C band-selective $\pi/2$ and π flip angle pulses except for the π pulses that should be band selective on the C^α region (Q3, 1200 μs) and for the adiabatic π pulse to invert both C' and C^α (smoothed chirp 500 μs, 20% smoothing, 80 kHz sweep width, 11.3 kHz radio frequency field strength) (45). An Eburp2 shape of duration of 1.768 ms and a Reburp shape of duration of 2.076 ms were used, respectively, for ^1H band-selective $\pi/2$ and π flip angle pulses. In the CON//HN experiment, solvent suppression was achieved through the 3:9:19 pulse scheme (46).

The ^{13}C band-selective pulses on C^α and C' were applied at the center of each region, respectively, and the ^1H-band-selective pulses were applied at the center of the H^N region at 8.13 ppm. Decoupling of $^{13}C^\alpha$ and ^{15}N was achieved with p5m4sp180 (Q3, 900 μs) and Waltz65 (100 μs) decoupling sequences, respectively (44,47). All gradients employed had a smoothed square shape.

All the spectra were acquired, processed, and analyzed by using Bruker TopSpin 4.0.1 software. Calibration of the spectra was achieved using 4,4-dimethyl-4-silapentane-1-sulfonic acid as a standard for ^1H and ^{13}C; ^{15}N shifts were calibrated indirectly (48).

The CON//HN was acquired with a CON interscan delay of 1.7 s; the HN was acquired within this delay. For each increment of the CON experiment, the in-phase (IP) and antiphase (AP) components were acquired and properly combined to achieve IPAP virtual decoupling (49) as described in Fig. S1. The CON spectrum was acquired with two scans, with sweep widths of 5555 Hz (^{13}C) × 2500 Hz (^{15}N) and 1024 × 512 real points in the two dimensions, respectively. The HN spectrum was acquired with 4 scans (2 scans as used for the CON × 2 additional scans because no IPAP decoupling is necessary for the HN), with sweep widths of 10,869 Hz (^1H) × 2000 Hz (^{15}N) and 1536 × 512 real points in the two dimensions, respectively. The total duration of the experiment was 1 h and 7 min. For comparison purposes, the two independent experiments with the same parameters were also acquired.

Similar parameters were used also for CON//HN experiments acquired for cell lysates and for in-cell samples as well as to follow the phosphorylation reaction, with the main difference being the use of four scans in the latter case because of lower sample concentration.

The CON//btNH was acquired with a CON interscan delay of 2.5 s; during this time, the btNH was repeated four times (recovery delay of 400 ms). For each increment of each experiment, the IP and AP components were acquired and properly combined to achieve IPAP virtual decoupling (49) as described in Fig. S2. The CON spectrum was acquired with 4 scans, with sweep widths of 5263 Hz ($^{13}C'$) × 2403 Hz (^{15}N) and 1024 × 1024 real points in the 2 dimensions, respectively. The btNH spectrum was acquired with 128 scans (4 scans as used for the CON × 4 repetitions of the btNH experiment × 8 because of the different number of increments needed in the indirect dimension), with sweep widths of 5263 Hz (^{15}N) × 2403 Hz (^1H) and 1024 × 128 real points in the two dimensions, respectively. The total duration of the experiment was 6 h and 19 min. For comparison purposes, the two independent experiments with the same parameters were also acquired.

The CON//(H)CAN was acquired with a CON interscan delay of 2.3 s; during this time, the (H)CAN was repeated three times (recovery delay of 700 ms). For each increment of each experiment, the IP and AP

components were acquired and properly combined to achieve IPAP virtual decoupling (49) as described in Fig. S3. The CON spectrum was acquired with 8 scans, with sweep widths of 5555 (^{13}C′) × 2554 Hz (^{15}N) and 1024 × 2048 real points in the two dimensions, respectively. The (H)CAN spectrum was acquired with 192 scans (8 scans as used for the CON × 3 repetitions of the (H)CAN experiment × 8 because of the different number of increments needed in the indirect dimension), with sweep widths of 5555 Hz (^{15}N) × 4000 Hz (^{13}C) and 1024 × 256 real points in the 2 dimensions, respectively. The total duration of the experiment was 60 h and 10 min. For comparison purposes, the two independent experiments with the same parameters were also acquired.

RESULTS AND DISCUSSION

The 2D CON has by now become one of the key experiments to characterize IDPs. Many experimental variants of the basic CON pulse sequence have been developed (43,50). Important features include the nuclear spins used as starting polarization source as well as the approach employed for homonuclear decoupling. When working with sample conditions approaching the "physiological" ones, like in the presence of high ionic strength, pH above 7, and relatively high temperature, the most preferred scheme is the simplest one, which starts on ^{13}C and actively exploits heteronuclear spins only. However, it requires a relaxation delay of ∼2 s to allow the C′ magnetization to relax back to equilibrium. Can we profitably use this delay to collect additional experiments?

The CON//HN experiment

The first two spectra generally collected on an IDP are the 2D HN and 2D CON. The experimental variant designed to acquire them simultaneously is here referred to as the CON//HN, and the spectra obtained on α-synuclein are shown in Fig. 1. The pulse sequence is reported in Fig. S1 and sketched in Fig. 1 *A*. In brief, a very simple logic was followed in the design of the pulse sequence. The CON experiment essentially exploits only two backbone nuclear spins (C′ and N). During the relaxation delay, an additional experiment can be acquired provided that different nuclear spins are perturbed and that it does not interfere with the CON itself. The ^{1}H-^{15}N heteronuclear single-quantum coherence (HSQC) exploits the amide proton as a starting polarization source as well as for acquisition of the FID; ^{15}N chemical shifts are sampled in the indirect dimension, just like in the CON experiment, and this does not cause any interference. Thus, it can be profitably acquired during the 2-s recycle delay of the CON. The only compromise to combine the two experiments derives from the need to decouple ^{15}N from ^{1}H and ^{13}C during the chemical shift evolution period. For the CON experiment, it is very important to use composite pulse decoupling of ^{1}H throughout the whole pulse sequence to minimize possible influence of exchange processes of amide protons with the solvent protons, which reduce signal intensities in particular when approaching physiological conditions. This does not constitute a problem because the ^{1}H-^{15}N HSQC pulse sequence precedes the CON one. Decoupling of ^{15}N from ^{13}C during the ^{15}N evolution period of the ^{1}H-^{15}N HSQC could be achieved by a combination of two 180° pulses in appropriate positions to restore C′ magnetization to equilibrium as a starting polarization source for the CON experiment. Thanks to this solution, the two spectra can be acquired simultaneously in the optimal conditions required for each of them as one can see by inspecting the quality of the spectra reported in Fig. 1. These were acquired on α-synuclein at 285 K and pH 6.5, which are conditions useful to evaluate whether all the expected resonances could be observed through the CON//HN experiment. Indeed, more than 99% of the backbone correlations could be detected in both experiments (133 out of 134 in the HN and 138 out of 139 in the CON, respectively).

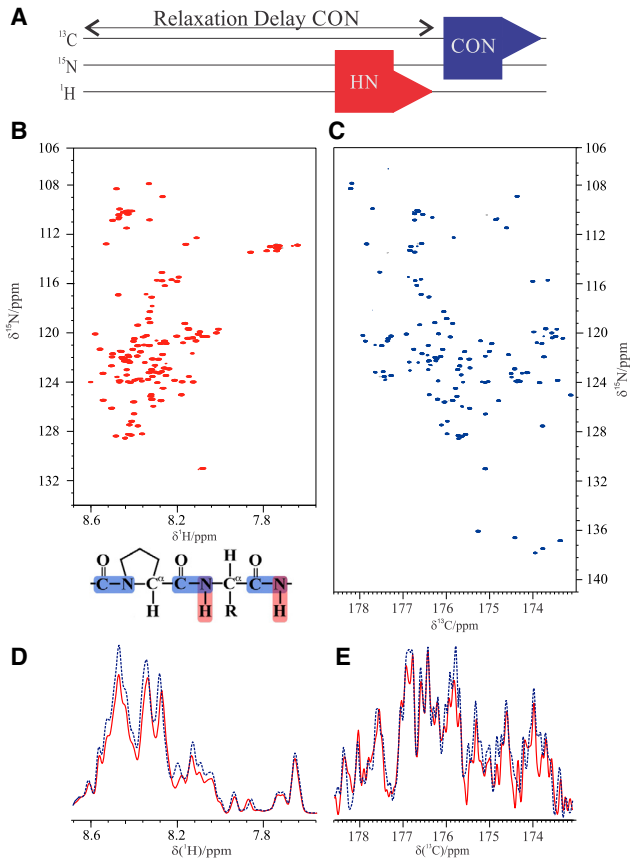

FIGURE 1 (*A*) Scheme of the CON//HN experiment. (*B*) HN and (*C*) CON 2D spectra acquired through the CON//HN experiment on ^{13}C, ^{15}N-labeled α-synuclein 1 mM at 285 K in 100 mM NaCl, 50 μM EDTA, and 20 mM phosphate buffer (pH 6.5) are shown. (*D*) A projection of the HN and the (*E*) CON spectra acquired with the CON//HN experiment (*red solid traces*) and with the corresponding experiments acquired independently (*blue dotted traces*) is shown. To see this figure in color, go online.

Comparison of the intensities of the spectra collected through the CON//HN experiment with those acquired with exactly the same parameters but in an independent fashion

shows that reduction in signal to noise ratio (S/N) resulting from the combination of the two experiments is minimal for the CON (5%) and more significant for the HN (15%) which, however, has an intrinsically higher sensitivity and provides the same number of peaks as the independent spectrum (Fig. 1, *D* and *E*).

When going to more demanding samples of limited lifetime, the advantages of recording the CON//HN are even more striking. The spectra acquired on α-synuclein in cell are shown in Fig. 2 *C* and are compared with those acquired on α-synuclein on cell lysates (Fig. 2 *B*) as well as on purified α-synuclein (Fig. 2 *A*) in conditions approaching physiological ones (310 K; pH 7.4). First of all, it is interesting to observe the spectra acquired on purified α-synuclein in these conditions and compare them with the analogous one acquired at lower pH and temperature (Fig. 1). The CON results are particularly useful to access complete information (138 detected backbone correlations; 99.3% of the expected ones); the quality of the HSQC is instead reduced because of increased solvent exchange broadening at higher pH and temperature (108 detected backbone correlations, 80.6% of the expected ones). Still, the two spectra provide interesting complementary information, including qualitative information about exchange processes.

The same spectra acquired on cell lysate show that most of the signals detected on the purified sample can be observed also in cell lysates. The possibility to acquire the two spectra simultaneously is very important, in particular for cell lysates, which have limited lifetimes. It is worth noting that the linewidths of the observed crosspeaks in the two spectra are very similar to those observed for purified α-synuclein, a nontrivial observation considering the complexity of cell lysate composition. When moving to in-cell experiments, the two spectra still show that a vast majority of the expected signals can be detected, providing atomic resolution information to characterize IDPs inside whole cells. However, the increase in linewidth when going to in-cell spectra is much more pronounced for the ^{1}H signals with respect to ^{13}C signals. Simultaneous acquisition of the two spectra is important to confirm that it is a real property of in-cell spectra and that it does not depend on possible changes in the experimental conditions or in-cell sample quality. Therefore, the CON//HN provides at the same time information derived from the exclusively heteronuclear spectra, characterized by narrow linewidths, as well as from proton-detected spectra, characterized by higher sensitivity but more influenced by line broadening deriving from both the inhomogeneous environment as well as from exchange processes.

The CON//^{15}N-detected experiments

^{15}N detection has interesting features for the study of IDPs because of the narrow linewidths and large dispersion of chemical shifts, provided one is in the appropriate sensitivity regime, which nowadays still requires highly

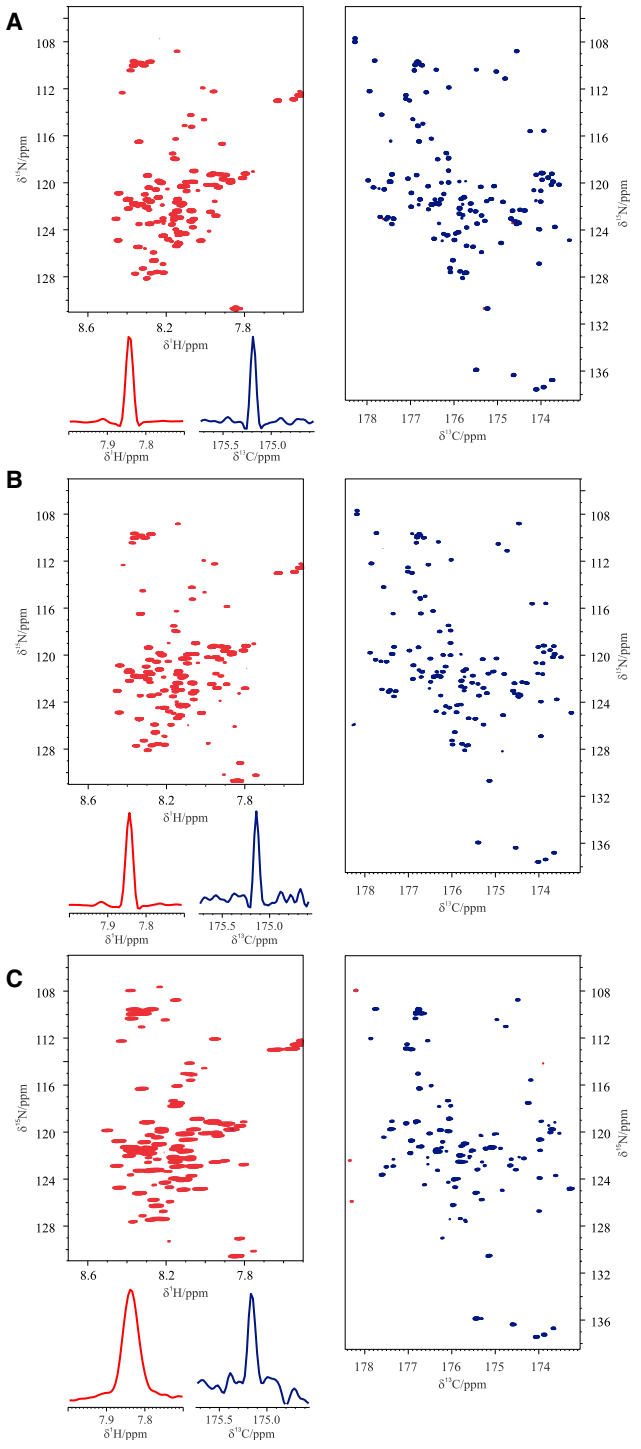

FIGURE 2 Comparison of the 2D spectra (HN *left*; CON *right*) acquired through the CON//HN experiment on ^{13}C, ^{15}N-labeled α-synuclein at 310 K in different experimental conditions: (*A*) purified sample in 100 mM NaCl, 50 μM EDTA, and 20 mM phosphate buffer at pH 7.4 is shown; (*B*) in *Escherichia coli* cells lysate resuspended in the same buffer as in (*A*) and (*C*) in-cell. The traces of a representative signal extracted from the HN (*red*; *left*) and the CON (*blue*; *right*) spectra are also reported. To see this figure in color, go online.

concentrated samples (30–33). The CON experiment was first combined with the ^{15}N-detected experiment to collect 2D HN spectra (CON//btNH) (51). The BEST-TROSY variant (52), which uses band-selective pulses for the amide protons, was selected to exploit the very efficient longitudinal relaxation enhancement of amide protons in IDPs (53–55) as well as to avoid ^{1}H decoupling during acquisition of the ^{15}N FID, two features that enable the acquisition of 3–4 ^{15}N FIDs during the CON relaxation delay to overcome the very low sensitivity of ^{15}N. Decoupling of ^{1}H during the ^{15}N evolution delay of the CON was achieved by pairs of 180° H^N band-selective pulses to restore the starting polarization source for the BEST-TROSY experiments. In addition, there is no proton decoupling during the acquisition of the CON. These two features reintroduce some dependence on solvent exchange processes as well as C'-H^N couplings in the direct acquisition dimension. The major modification included in the BEST-TROSY part of the experiment was to avoid composite pulse decoupling of carbonyl carbon nuclear spins during the acquisition of the ^{15}N FID to preserve C' polarization for the following CON experiment. To this end, virtual decoupling of C' during the acquisition of the ^{15}N FID was implemented through the IPAP approach (56) in combination with band-selective decoupling of the C^{α} spins. The pulse sequence is reported in Fig. S2 and schematically illustrated in Fig. 3 *A*. The results of the CON//btNH experiments recorded on α-synuclein at different temperatures are reported in Fig. 3, B and C. The good performance of the experiment is shown by the well-resolved spectra that can be acquired; essentially all expected correlations can be detected at 285 K and pH 6.5 (138 detected backbone correlations for the CON and 133 for the btNH; 99.3% of the expected ones for each spectrum). The modifications introduced to acquire the two spectra simultaneously slightly reduce the sensitivity of the CON spectrum, which is, however, the more sensitive of the two and thus only has a minor impact on the final outcome (Fig. 3, *D* and *E*). The ^{15}N-detected BEST-TROSY HN spectrum, although less influenced by exchange broadening of amide protons than its ^{1}H-detected counterpart, still relies on amide protons in the initial coherence transfer step as well as in the ^{1}H chemical shift evolution achieved in the indirect dimension. As expected, with increasing temperature, the quality of the CON is essentially maintained, whereas the intensity of crosspeaks in the ^{15}N-detected BEST-TROSY spectrum is reduced. Still, it can be observed that even at higher temperature than physiological one (315 K), a few additional crosspeaks can be observed in the ^{15}N-detected BEST-TROSY HN spectrum that were not identified in these conditions through ^{1}H-detected experiments (Biological Magnetic Resonance Bank [BMRB]: 27348) (57). In particular, in the ^{1}H-detected experiment, 93/134 peaks were visible, whereas when performing the ^{15}N-detected variant, seven additional peaks are visible (thus 100/134), mostly due to polar residues (Thr-22, -64, -44, -33, Ser-9, Lys-43, Ala-76). Even if the signal intensity is lower in the ^{15}N-detected experiment because of the lower gyromagnetic ratio of ^{15}N, it is possible to collect a few more signals because the proton magnetization is transverse for a shorter amount of time,

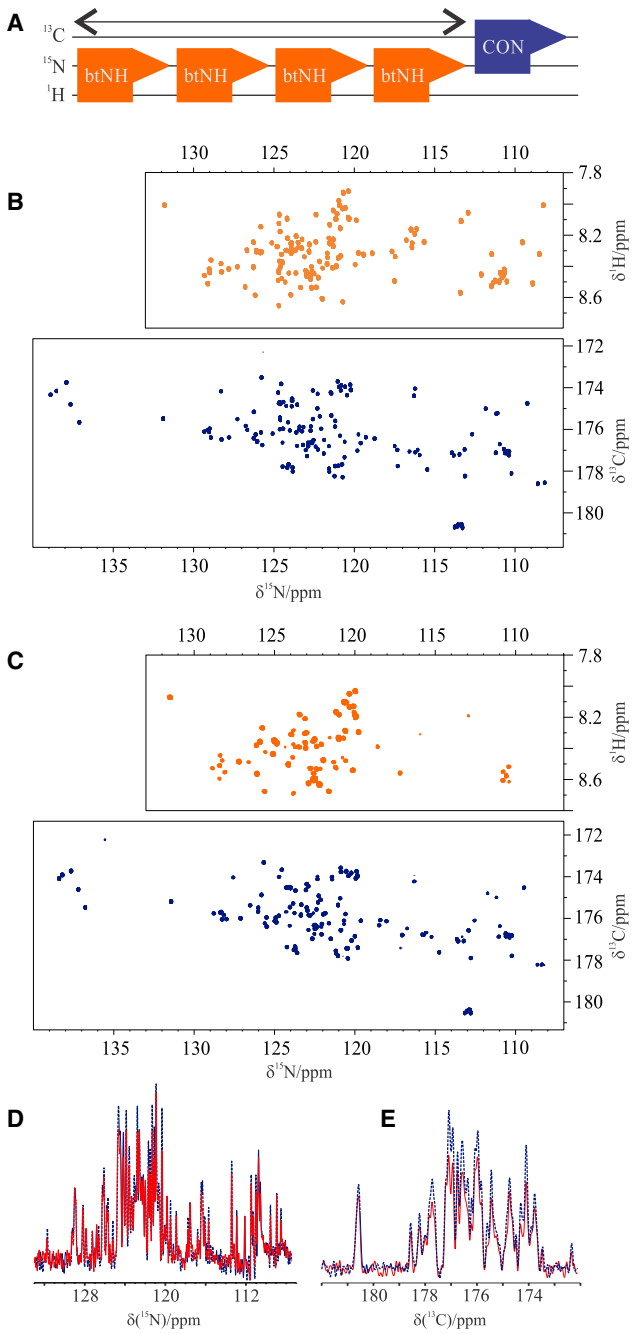

FIGURE 3 (*A*) Scheme of the CON//btNH experiment. The 2D spectra (btNH *top*; CON *bottom*) acquired with the CON//btNH experiment on ^{13}C,^{15}N-labeled α-synuclein 1 mM at (*B*) 285 K and (*C*) 315 K at pH 6.5 in the same buffer reported in Fig. 1 are shown. (*D*) and (*E*) report the comparison of the S/N of the projection of the spectra acquired with the CON//btNH experiment (*red solid traces*) with the analogous spectra acquired independently (*blue dotted traces*). To see this figure in color, go online.

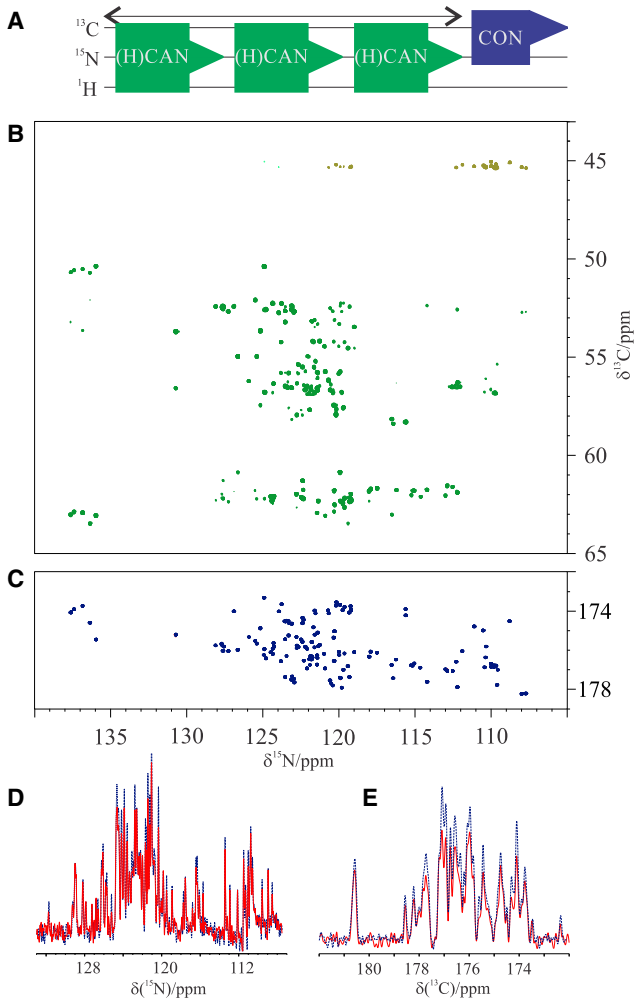

FIGURE 4 (*A*) Scheme of the CON//(H)CAN experiment. (*B*) (H)CAN and (*C*) CON spectra recorded on ^{13}C, ^{15}N-labeled α-synuclein at 310 K (pH 7.4) are shown. (*D*) and (*E*) report the comparison of the S/N of the projection of the spectra acquired with the CON//(H)CAN experiment (*red solid traces*) with the analogous spectra acquired independently (*blue dotted traces*). To see this figure in color, go online.

reducing losses. This shows that the method has some potential, in particular using optimized hardware (high fields and optimized probes). Another experiment based on ^{15}N detection that was combined with the CON is the (H)CAN (58). The CON//(H)CAN acquired at 310 K and pH 7.4 is shown in Fig. 4. The pulse sequence is reported in Fig. S3 and schematically illustrated in Fig. 4 *A*. As for the previous experiment, this magnetization transfer pathway starts from a proton, the H^{α}, and is then transferred to the C^{α}. The C^{α} dimension evolves as the indirect one. The magnetization can now be transferred to N of the same amino acid, through the ^{1}J constant, and to the previous one, through the ^{2}J constant. The two constants are similar and it is thus difficult to distinguish one pathway from the other. However, we decided to prioritize the intraresidue correlations, which are more sensitive and provide complementary information, with respect to the one available through the CON experiment. When exploiting H^{α} as starting polarization source, the results are optimal at any temperature because of the nonexchangeable property of this atom. Longitudinal relaxation enhancements are expected to be modest for H^{α} in IDPs (55), and thus nonselective ^{1}H pulses can be used. More than one repetition of this experiment during the CON relaxation delay can be collected thanks to the relatively short time needed for H^{α} to recover to the steady state (hundreds of milliseconds). Technical compromises needed in this case are very similar to those discussed for the previous experiment. They are responsible for a small reduction in the sensitivity of the CON (Fig. 4, *D* and *E*), which, however, is the more sensitive between the two. Decoupling of ^{1}H and ^{13}C was achieved by pairs of 180° pulses to restore the magnetization to equilibrium for subsequent experiments. For the same reason, a virtual CO decoupling scheme is required for the acquisition of ^{15}N FIDs. To this end, we implemented the IPAP scheme, in combination with band-selective decoupling of the C^{α} spins.

In this spectrum, all the correlations of the intraresidue crosspeaks are observed as well as part of the interresidue ones (113/139; 81.0%). However, significant overlap still occurs, and only a fraction of them are resolved. It is worth noting however that with increasing magnetic fields and with tailored probes, the CON//(H)CAN becomes a promising tool for the study of IDPs. Finally, should long experimental times be necessary to compensate for a lower ^{15}N sensitivity, the CON//(H)CAN experiment can reveal weak crosspeaks present in the CON such as those deriving from the *cis-trans* proline isomerization, which has not been extensively studied for IDPs and has been found to be important in many regulatory processes.

Comparison with other methods

Here, we have chosen to opt for the most straightforward approach to combine two experiments: instead of simply waiting for the magnetization to recover before the next transient, we use the recovery delay of one particularly useful experiment, which would be acquired anyway, to collect an additional one providing complementary information for free. This method follows the idea of activating unexploited magnetization (UTOPIA) (34) but shifts the central interest to the ^{13}C-detected experiment, as schematically indicated in Fig. 1. The simplest variant of the CON experiment was selected because it represents the most robust one to ensure detection of all signals of an IDP near physiological conditions, including those that are invisible in HN spectra (residues experiencing fast solvent exchange and proline residues). This was combined either with ^{1}H-detected or with ^{15}N-detected 2D experiments.

In principle, a 3D HNCO (or a 3D HNCA), which can nowadays be collected in a very quick time thanks to projection spectroscopy (59) or nonuniform acquisition and processing strategies (60,61), could provide very similar

information. However, the results of these 3D spectra depend on the observability of amide protons. Therefore, the approach presented here is more suitable to study IDPs approaching physiological conditions (310 K; pH 7.4; ionic strength value around 0.25 M; in-cell environment) because the CON is not affected by fast solvent exchange processes.

Similar arguments hold when comparing the current approach with an elegant experimental variant of the HNCO proposed for parallel acquisition of the HN and (H^N)CON experiments (33). In this case, the two spectra (HN and (H^N)CON) are obtained by recovering magnetization from two different pathways that however both originate from H^N polarization. As a result, the two spectra are influenced by solvent exchange broadening, and the (H^N)CON does not reveal proline signals.

The relative sensitivity of the two experiments to be combined is an important issue to be considered. There is no doubt that the intrinsic sensitivity of ^{13}C is lower than that of ^{1}H because of the lower gyromagnetic ratio. However, thanks to instrumental improvements, the sensitivity of the CON experiments acquired on highly flexible IDPs is sufficient to collect the experiment with just a few scans per increment. Therefore, it is worth combining it with the other experiment that is generally collected on an IDP, the HN correlation spectrum. The relative sensitivity of the two experiments is inverted when combining the CON with ^{15}N-detected experiments. This difference can be partly compensated by exploiting ^{1}H as a starting polarization source, exploiting longitudinal relaxation enhancement (when possible) (49,51,52,55), or accumulating more ^{15}N FIDs. A leap in instrumental sensitivity exploiting dedicated probe heads will provide the necessary push to make this combination of experiments really amenable for every application.

From this analysis, it is clear that more than for time savings, which are generally moderate when considering combinations of simple 2D experiments, the simultaneous acquisition of two spectra is important for accessing a snapshot of an IDP in cases in which the sample either has limited stability in time or it changes because of chemical reactions as it happens when studying posttranslational modifications (PTMs). In these cases, to investigate the IDP of interest, in addition to the CON one can access complementary information through the multiple receiver CON variants proposed here.

A case study for PTMs

PTMs represent the most efficient way to modulate the biological activity of proteins after their biosynthesis through chemical reactions, catalyzed by enzymes. Indeed, it is possible to modulate the chemo-physical properties of a protein and thus its function by adding or removing specific chemical groups or through the cleavage of chemical bonds. The diversity of PTMs found in proteins arises from the very different processes that they can modulate in a cell such as protein folding, signaling, molecular recognition, interactions, and degradation. In this way, the same protein can be handled for different aims, ranging from cell fate control to regulation of metabolism (62).

IDPs are frequently involved in regulatory and signaling functions, which can be modulated by PTMs (63–65). PTMs can trigger both local and long-range changes as well as intermolecular interactions. It has been supposed that structural flexibility could also be a biological strategy to overcome the classical problem of the "one lock/one key" model. The lack of a stable 3D structure guarantees adaptability for the enzymatic site and allows high specificity of the process, maintaining, however, low affinity (64,66).

Among a variety of possible modifications, one of the most common is phosphorylation. It was estimated that at least 2% of the human genome is constituted by kinases and more than 30% of the eukaryotic proteins are involved in phosphorylation, with 700,000 sites that can potentially act as substrates (67). Investigating this mechanism is fundamental to understand functions of these important enzymes. PTMs usually involve only a few residues, and NMR provides a unique tool to study these processes, giving access to residue-specific atomic resolution information.

It is well known that the role of some IDPs or IDRs and their link to the onset of several diseases is strictly dependent on PTMs, as phosphorylation (64–66,68). A clear example is the supposed key role of phosphorylation of specific α-synuclein residues in the modulation of Lewy bodies formation. In this widely studied process, serine 129 is selectively and extensively phosphorylated, promoting fibrillation in vitro (69–71). It has emerged that this process occurs together with phosphorylation of tyrosine 125, a priming event in the efficient modification of serine 129 by CK1 kinase, both in vitro under physiological conditions and in vivo (72–74).

To provide an example of the utility of the CON//HN experiment, we show here the phosphorylation reaction of tyrosine residues by Fyn near physiological conditions. Fyn is a nonreceptor tyrosine kinase of the Src family that has been shown to react with all the four tyrosine residues present in α-synuclein (Y39, Y125, Y133, Y136) with high-percentage levels but preferentially targeting Y125. The spectra acquired with the CON//HN experiment during the phosphorylation reaction are shown in Fig. 5. It can be observed that the changes in HN crosspeaks agree with previous observations (73) and that additional details are monitored through the CON spectrum acquired simultaneously (Fig. 5). In particular, the CON spectrum, which exploits the ^{13}C in the direct dimension, has a higher resolution with respect to the HN spectrum. Thus, we can also monitor the shift of those peaks, which, in the HN spectrum, are

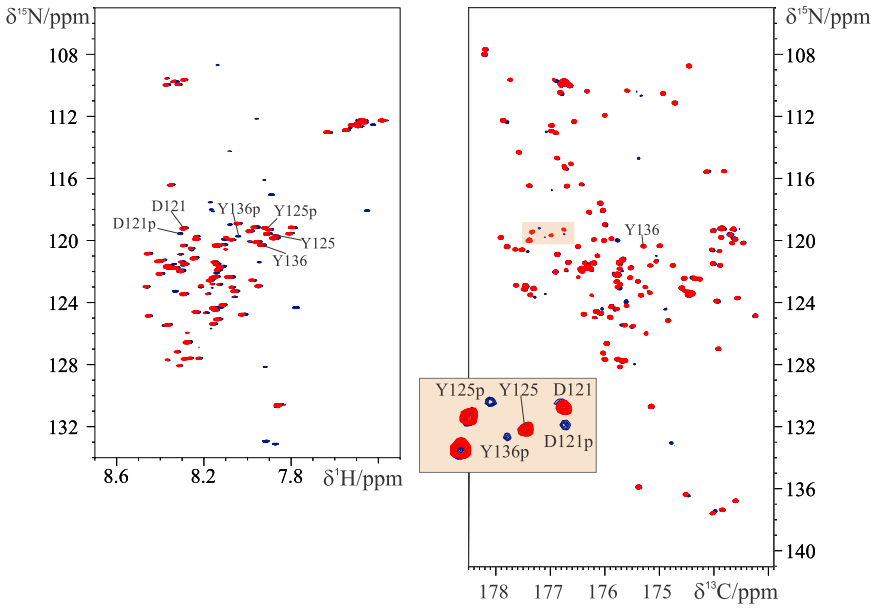

FIGURE 5 The 2D spectra acquired with the CON//HN experiment to monitor phosphorylation of ^{13}C, ^{15}N-labeled α-synuclein 200 μM with Fyn tyrosine kinase as a function of time ($t = 0$ h, *red spectra*; $t = 50$ h *blue spectra*). The HN spectra are reported on the left and the CON on the right. The highlighted region of the CON spectra is enlarged to show, as an example, a subset of α-synuclein signals that are influenced by phosphorylation. The reaction was performed at 303 K in 20 mM phosphate buffer, 100 mM NaCl, 50 μM EDTA, 2 mM dithiothreitol, 6 mM $MgCl_2$, and 3 mM ATP (pH 7.0). To see this figure in color, go online.

found in crowded regions such as those of Tyr125, which is well resolved in the CON (Fig. 5).

A final comment is necessary on the specific conditions needed to follow PTMs. Most enzymes indeed fulfill their roles at physiological conditions. Therefore, the CON//HN experiment offers a particularly useful tool because in addition to the HN, often used to study PTMs, it exploits the CON, which is not influenced by exchange broadening because of the chemical properties of the nuclei participating in the magnetization transfer pathway. The fairly low substrate concentration generally required for these reactions is still sufficient to acquire good quality ^{13}C-detected spectra, demonstrating the general applicability of this approach.

CONCLUSION

Research in the area of IDPs is continuously expanding. Partly or completely disordered proteins of increasing size and complexity and with high biomedical relevance are being discovered at fast pace, adding a novel layer to structural biology. In this frame, NMR spectroscopy has a central role, enabling the investigation of systems of increasing complexity in an environment that resembles more and more the physiological one. Heteronuclear direct detection has contributed to establishing the importance of NMR in this area of research. The possibility to collect two spectra simultaneously is very attractive to study IDPs. Several experimental variants are presented here in which during the recovery delay needed to acquire the CON, an additional 2D spectrum is collected either based on ^{1}H detection (CON//HN) or on ^{15}N detection (CON//btNH, CON//(H)CAN). This, to our knowledge, novel approach is particularly useful to study samples of limited lifetime, such as IDPs inside whole cells or cell lysates, as well as to follow chemical reactions such as PTMs of IDPs in conditions approaching physiological ones (pH, temperature, ionic strength, inhomogeneous in-cell environment). The availability of cryogenically cooled probeheads optimized for heteronuclear direct detection is important to alleviate the problem of the intrinsic lower sensitivity of heteronuclei. The usefulness of these experiments is bound to increase with increasing magnetic fields to take maximal advantage of the narrow linewidths of C′ and N of highly flexible IDPs, enabling the study of IDPs of increasing complexity.

SUPPORTING MATERIAL

Supporting Material can be found online at https://doi.org/10.1016/j.bpj.2019.05.017.

AUTHOR CONTRIBUTIONS

I.C.F. and R.P. designed the research. All the authors performed research, analyzed the data, discussed the results, and wrote the manuscript.

ACKNOWLEDGMENTS

The support and the use of resources of the CERM/CIRMMP center of Instruct-ERIC, a Landmark European Strategy Forum on Research Infrastructures project, is gratefully acknowledged. Dr. F. X. Theillet, and Dr. A. Binolfi are gratefully acknowledged for the stimulating discussions.

This work has been supported in part by a grant from the Fondazione CR Firenze and by a grant from the Italian Ministry of Foreign Affairs and International Cooperation (MAE0057283) to R.P.

REFERENCES

1. Habchi, J., P. Tompa, …, V. N. Uversky. 2014. Introducing protein intrinsic disorder. *Chem. Rev.* 114:6561–6588.

2. Wright, P. E., and H. J. Dyson. 2015. Intrinsically disordered proteins in cellular signalling and regulation. *Nat. Rev. Mol. Cell Biol.* 16:18–29.
3. van der Lee, R., M. Buljan, …, M. M. Babu. 2014. Classification of intrinsically disordered regions and proteins. *Chem. Rev.* 114:6589–6631.
4. Uversky, V. N., C. J. Oldfield, and A. K. Dunker. 2008. Intrinsically disordered proteins in human diseases: introducing the D2 concept. *Annu. Rev. Biophys.* 37:215–246.
5. Ambadipudi, S., and M. Zweckstetter. 2016. Targeting intrinsically disordered proteins in rational drug discovery. *Expert Opin. Drug Discov.* 11:65–77.
6. Joshi, P., S. Chia, …, M. Vendruscolo. 2016. A fragment-based method of creating small-molecule libraries to target the aggregation of intrinsically disordered proteins. *ACS Comb. Sci.* 18:144–153.
7. Heller, G. T., F. A. Aprile, and M. Vendruscolo. 2017. Methods of probing the interactions between small molecules and disordered proteins. *Cell. Mol. Life Sci.* 74:3225–3243.
8. Tsafou, K., P. B. Tiwari, …, J. A. Toretsky. 2018. Targeting intrinsically disordered transcription factors: changing the paradigm. *J. Mol. Biol.* 430:2321–2341.
9. Eliezer, D. 2009. Biophysical characterization of intrinsically disordered proteins. *Curr. Opin. Struct. Biol.* 19:23–30.
10. I. C. Felli and R. Pierattelli, eds 2015. Intrinsically Disordered Proteins Studied by NMR Spectroscopy Springer, Basel, Switzerland.
11. Gil, S., T. Hošek, …, I. C. Felli. 2013. NMR spectroscopic studies of intrinsically disordered proteins at near-physiological conditions. *Angew. Chem. Int. Ed. Engl.* 52:11808–11812.
12. Dyson, H. J., and P. E. Wright. 2001. Nuclear magnetic resonance methods for elucidation of structure and dynamics in disordered states. *Methods Enzymol.* 339:258–270.
13. Konrat, R. 2014. NMR contributions to structural dynamics studies of intrinsically disordered proteins. *J. Magn. Reson.* 241:74–85.
14. Brutscher, B., I. C. Felli, …, Z. Sólyom. 2015. NMR methods for the study of instrinsically disordered proteins structure, dynamics, and interactions: general overview and practical guidelines. *Adv. Exp. Med. Biol.* 870:49–122.
15. Bermel, W., I. Bertini, …, R. Pierattelli. 2006. Protonless NMR experiments for sequence-specific assignment of backbone nuclei in unfolded proteins. *J. Am. Chem. Soc.* 128:3918–3919.
16. Bermel, W., I. Bertini, …, R. Pierattelli. 2006. Novel ^{13}C direct detection experiments, including extension to the third dimension, to perform the complete assignment of proteins. *J. Magn. Reson.* 178:56–64.
17. Pérez, Y., M. Gairí, …, P. Bernadó. 2009. Structural characterization of the natively unfolded N-terminal domain of human c-Src kinase: insights into the role of phosphorylation of the unique domain. *J. Mol. Biol.* 391:136–148.
18. Knoblich, K., S. Whittaker, …, U. Günther. 2009. Backbone assignment of the N-terminal polyomavirus large T antigen. *Biomol. NMR Assign.* 3:119–123.
19. Contreras-Martos, S., A. Piai, …, P. Tompa. 2017. Linking functions: an additional role for an intrinsically disordered linker domain in the transcriptional coactivator CBP. *Sci. Rep.* 7:4676.
20. Hošek, T., E. O. Calçada, …, R. Pierattelli. 2016. Structural and dynamic characterization of the molecular hub early region 1A (E1A) from human adenovirus. *Chemistry.* 22:13010–13013.
21. Motáčková, V., J. Nováček, …, V. Sklenář. 2010. Strategy for complete NMR assignment of disordered proteins with highly repetitive sequences based on resolution-enhanced 5D experiments. *J. Biomol. NMR.* 48:169–177.
22. Haba, N. Y., R. Gross, …, J. H. Chill. 2013. NMR determines transient structure and dynamics in the disordered C-terminal domain of WASp interacting protein. *Biophys. J.* 105:481–493.
23. Nováček, J., N. Y. Haba, …, V. Sklenář. 2012. 4D non-uniformly sampled HCBCACON and ^{1}J(NCα)-selective HCBCANCO experiments for the sequential assignment and chemical shift analysis of intrinsically disordered proteins. *J. Biomol. NMR.* 53:139–148.
24. Lawrence, C. W., and S. A. Showalter. 2012. Carbon-detected ^{15}N NMR spin relaxation of an intrinsically disordered protein: FCP1 dynamics unbound and in complex with RAP74. *J. Phys. Chem. Lett.* 3:1409–1413.
25. Sahu, D., M. Bastidas, and S. A. Showalter. 2014. Generating NMR chemical shift assignments of intrinsically disordered proteins using carbon-detected NMR methods. *Anal. Biochem.* 449:17–25.
26. Lopez, J., R. Schneider, …, G. Lippens. 2016. Studying intrinsically disordered proteins under true in vivo conditions by combined cross-polarization and carbonyl-detection NMR spectroscopy. *Angew. Chem. Int.Engl.* 55:7418–7422.
27. Piai, A., E. O. Calçada, …, R. Pierattelli. 2016. Just a flexible linker? The structural and dynamic properties of CBP-ID4 revealed by NMR spectroscopy. *Biophys. J.* 110:372–381.
28. Eftekharzadeh, B., A. Piai, …, X. Salvatella. 2016. Sequence context influences the structure and aggregation behavior of a PolyQ tract. *Biophys. J.* 110:2361–2366.
29. Kovacs, H., D. Moskau, and M. Spraul. 2005. Cryogenically cooled probes - a leap in NMR technology. *Prog. Nucl. Mag. Res. Sp.* 46:131–155.
30. Takeuchi, K., G. Heffron, …, G. Wagner. 2010. Nitrogen-detected CAN and CON experiments as alternative experiments for main chain NMR resonance assignments. *J. Biomol. NMR.* 47:271–282.
31. Takeuchi, K., H. Arthanari, and G. Wagner. 2016. Perspective: revisiting the field dependence of TROSY sensitivity. *J. Biomol. NMR.* 66:221–225.
32. Chhabra, S., P. Fischer, …, H. Arthanari. 2018. ^{15}N detection harnesses the slow relaxation property of nitrogen: delivering enhanced resolution for intrinsically disordered proteins. *Proc. Nat. Acad. Sci. USA.* 115:1710–1719.
33. Gibbs, E. B., and R. W. Kriwacki. 2018. Direct detection of carbon and nitrogen nuclei for high-resolution analysis of intrinsically disordered proteins using NMR spectroscopy. *Methods.* 138-139:39–46.
34. Kupče, E., R. Freeman, and B. K. John. 2006. Parallel acquisition of two-dimensional NMR spectra of several nuclear species. *J. Am. Chem. Soc.* 128:9606–9607.
35. Kupče, E., and R. Freeman. 2010. Molecular structure from a single NMR sequence (fast-PANACEA). *J. Magn. Reson.* 206:147–153.
36. Chakraborty, S., S. Paul, and R. V. Hosur. 2012. Simultaneous acquisition of $^{13}C^{\alpha}$-^{15}N and ^{1}H-^{15}N-^{15}N sequential correlations in proteins: application of dual receivers in 3D HNN. *J. Biomol. NMR.* 52:5–10.
37. Kupče, E., and L. E. Kay. 2012. Parallel acquisition of multi-dimensional spectra in protein NMR. *J. Biomol. NMR.* 54:1–7.
38. Viegas, A., T. Viennet, …, M. Etzkorn. 2016. UTOPIA NMR: activating unexploited magnetization using interleaved low-gamma detection. *J. Biomol. NMR.* 64:9–15.
39. Kupče, E. 2013. NMR with multiple receivers. *Top. Curr. Chem.* 335:71–96.
40. Sharma, K., P. K. Madhu, and K. R. Mote. 2016. A suite of pulse sequences based on multiple sequential acquisitions at one and two radio-frequency channels for solid-state magic-angle spinning NMR studies of proteins. *J. Biomol. NMR.* 65:127–141.
41. Kupče, Ē., L. E. Kay, and R. Freeman. 2010. Detecting the "afterglow" of ^{13}C NMR in proteins using multiple receivers. *J. Am. Chem. Soc.* 132:18008–18011.
42. Huang, C., G. Ren, …, C. C. Wang. 2005. A new method for purification of recombinant human α-synuclein in *Escherichia coli*. *Protein Expr. Purif.* 42:173–177.
43. Felli, I. C., L. Gonnelli, and R. Pierattelli. 2014. In-cell ^{13}C NMR spectroscopy for the study of intrinsically disordered proteins. *Nat. Protoc.* 9:2005–2016.
44. Emsley, L., and G. Bodenhausen. 1992. Optimization of shaped selective pulses for NMR using a quaternion description of their overall propagators. *J. Magn. Reson.* 97:135–148.

45. Böhlen, J. M., and G. Bodenhausen. 1993. Experimental aspects of Chirp NMR spectroscopy. *J. Magn. Reson.* 102:293–301.

46. Piotto, M., V. Saudek, and V. Sklenár. 1992. Gradient-tailored excitation for single-quantum NMR spectroscopy of aqueous solutions. *J. Biomol. NMR.* 2:661–665.

47. Freeman, R., and H. Geen. 1991. Band-selective radiofrequency pulses. *J. Magn. Reson.* 93:93–141.

48. Markley, J. L., A. Bax, …, K. Wüthrich. 1998. Recommendations for the presentation of NMR structures of proteins and nucleic acids. *Pure Appl. Chem.* 70:117–142.

49. Felli, I. C., and R. Pierattelli. 2015. Spin-state-selective methods in solution- and solid-state biomolecular ^{13}C NMR. *Prog. Nucl. Magn. Reson. Spectrosc.* 84–85:1–13.

50. Felli, I. C., and R. Pierattelli. 2014. Novel methods based on ^{13}C detection to study intrinsically disordered proteins. *J. Magn. Reson.* 241:115–125.

51. Takeuchi, K., H. Arthanari, …, G. Wagner. 2015. Nitrogen detected TROSY at high field yields high resolution and sensitivity for protein NMR. *J. Biomol. NMR.* 63:323–331.

52. Solyom, Z., M. Schwarten, …, B. Brutscher. 2013. BEST-TROSY experiments for time-efficient sequential resonance assignment of large disordered proteins. *J. Biomol. NMR.* 55:311–321.

53. Schanda, P., V. Forge, and B. Brutscher. 2006. HET-SOFAST NMR for fast detection of structural compactness and heterogeneity along polypeptide chains. *Magn. Reson. Chem.* 44:S177–S184.

54. Schanda, P., H. Van Melckebeke, and B. Brutscher. 2006. Speeding up three-dimensional protein NMR experiments to a few minutes. *J. Am. Chem. Soc.* 128:9042–9043.

55. Hošek, T., S. Gil-Caballero, …, I. C. Felli. 2015. Longitudinal relaxation properties of $^{1}H^{N}$ and $^{1}H^{\alpha}$ determined by direct-detected ^{13}C NMR experiments to study intrinsically disordered proteins (IDPs). *J. Magn. Reson.* 254:19–26.

56. Bermel, W., I. Bertini, …, R. Pierattelli. 2006. ^{13}C-detected protonless NMR spectroscopy of proteins in solution. *Prog. Nucl. Mag. Res. Sp.* 48:25–45.

57. Murrali, M. G., M. Schiavina, …, I. C. Felli. 2018. ^{13}C APSY-NMR for sequential assignment of intrinsically disordered proteins. *J. Biomol. NMR.* 70:167–175.

58. Gal, M., K. A. Edmonds, …, G. Wagner. 2011. Speeding up direct ^{15}N detection: hCaN 2D NMR experiment. *J. Biomol. NMR.* 51:497–504.

59. Hiller, S., F. Fiorito, …, G. Wider. 2005. Automated projection spectroscopy (APSY). *Proc. Natl. Acad. Sci. USA.* 102:10876–10881.

60. Robson, S., H. Arthanari, …, G. Wagner. 2019. Nonuniform sampling for NMR spectroscopy. *Methods Enzymol.* 614:263–291.

61. Kazimierczuk, K., J. Stanek, …, W. Koźmiński. 2010. Random sampling in multidimensional NMR spectroscopy. *Prog. Nucl. Magn. Reson. Spectrosc.* 57:420–434.

62. Cheng, H. C., R. Z. Qi, …, H. J. Zhu. 2011. Regulation and function of protein kinases and phosphatases. *Enzyme Res.* 2011:794089.

63. Zhou, J., S. Zhao, and A. K. Dunker. 2018. Intrinsically disordered proteins link alternative splicing and post-translational modifications to complex cell signaling and regulation. *J. Mol. Biol.* 430:2342–2359.

64. Darling, A. L., and V. N. Uversky. 2018. Intrinsic disorder and post-translational modifications: the darker side of the biological dark matter. *Front. Genet.* 9:158.

65. Bah, A., and J. D. Forman-Kay. 2016. Modulation of intrinsically disordered protein function by post-translational modifications. *J. Biol. Chem.* 291:6696–6705.

66. Uversky, V. N. 2014. Wrecked regulation of intrinsically disordered proteins in diseases: pathogenicity of deregulated regulators. *Front. Mol. Biosci.* 1:6.

67. Ubersax, J. A., and J. E. Ferrell, Jr. 2007. Mechanisms of specificity in protein phosphorylation. *Nat. Rev. Mol. Cell Biol.* 8:530–541.

68. Fujiwara, H., M. Hasegawa, …, T. Iwatsubo. 2002. α-synuclein is phosphorylated in synucleinopathy lesions. *Nat. Cell Biol.* 4:160–164.

69. Choi, H. S., H. Liew, …, Y. H. Suh. 2012. Phosphorylation of α-synuclein is crucial in compensating for proteasomal dysfunction. *Biochem. Biophys. Res. Commun.* 424:597–603.

70. Mahul-Mellier, A. L., B. Fauvet, …, H. A. Lashuel. 2014. c-Abl phosphorylates α-synuclein and regulates its degradation: implication for α-synuclein clearance and contribution to the pathogenesis of Parkinson's disease. *Hum. Mol. Genet.* 23:2858–2879.

71. Schmid, A. W., B. Fauvet, …, H. A. Lashuel. 2013. α-synuclein post-translational modifications as potential biomarkers for Parkinson disease and other synucleinopathies. *Mol. Cell. Proteomics.* 12:3543–3558.

72. Nakamura, T., H. Yamashita, …, S. Nakamura. 2001. Activated Fyn phosphorylates α-synuclein at tyrosine residue 125. *Biochem. Biophys. Res. Commun.* 280:1085–1092.

73. Kosten, J., A. Binolfi, …, P. Selenko. 2014. Efficient modification of α-synuclein serine 129 by protein kinase CK1 requires phosphorylation of tyrosine 125 as a priming event. *ACS Chem. Neurosci.* 5:1203–1208.

74. Paleologou, K. E., A. W. Schmid, …, H. A. Lashuel. 2008. Phosphorylation at Ser-129 but not the phosphomimics S129E/D inhibits the fibrillation of α-synuclein. *J. Biol. Chem.* 283:16895–16905.

Biophysical Journal, Volume *117*

Supplemental Information

Taking Simultaneous Snapshots of Intrinsically Disordered Proteins in Action

Marco Schiavina, Maria Grazia Murrali, Letizia Pontoriero, Valerio Sainati, Rainer Kümmerle, Wolfgang Bermel, Roberta Pierattelli, and Isabella C. Felli

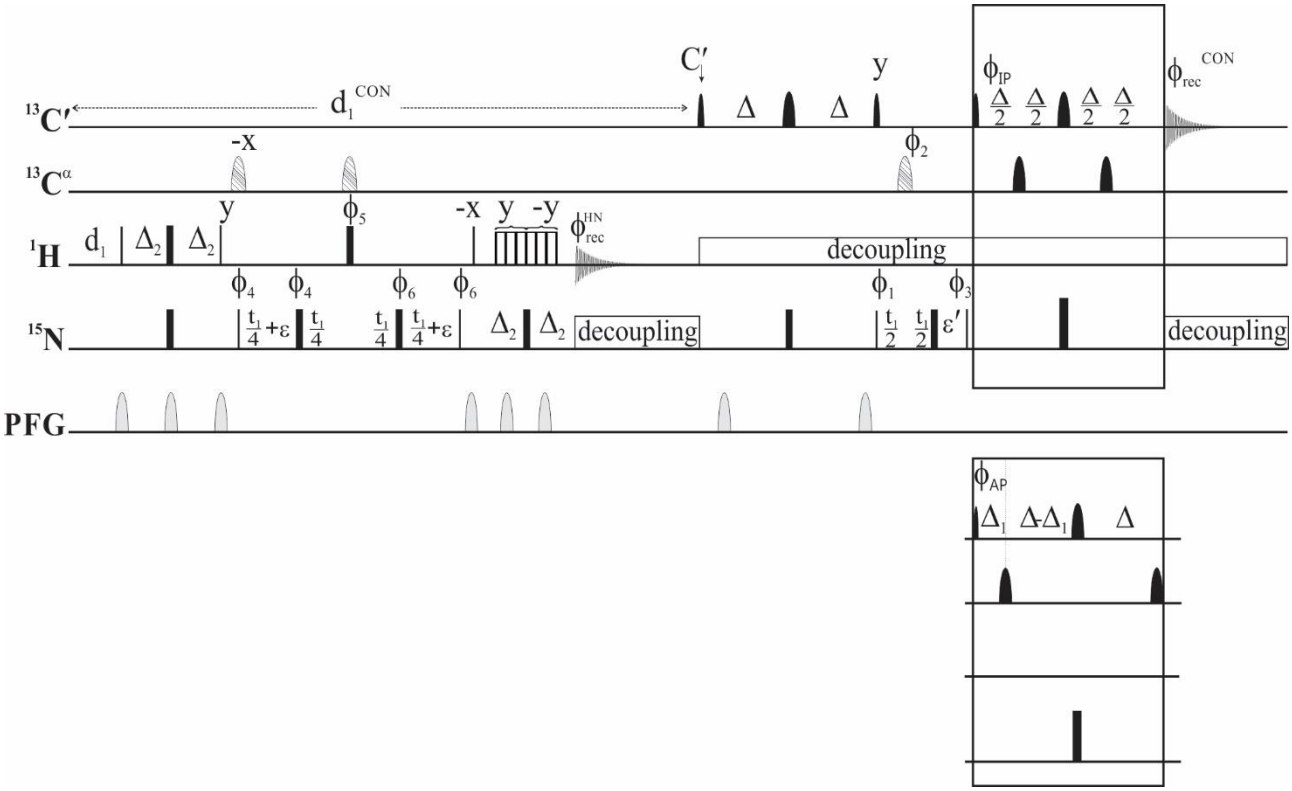

Figure S1. CON//HN pulse sequence scheme.

Narrow and wide black rectangles represent $\pi/2$ and π non-selective pulses; narrow and wide black symbols represent $\pi/2$ and π band-selective pulses (Q5 and Q3 shapes of 300 and 231 µs respectively), hatched pulses are adiabatic inversion pulse on C′ and C^{α} (smoothed Chirp 500 µs 80 kHz sweep and 20% smooting).

The following phase cycling was employed for the CON//HN: ϕ_1 = x, -x ; ϕ_2 = 2(x), 2(-x); ϕ_3 = 4(x), 4(-x), ϕ^{IP} = x ; ϕ^{AP} = -y and $\phi_{rec}{}^{CON}$= x, -x, x, -x, -x, x, -x, x for the 2D-CON and ϕ_4 = x, –x, ϕ_5 = 2(x), 2(-x) ϕ_6 = 4(x) 4(-x) and $\phi_{rec}{}^{HN}$ = x, -x, x, -x, -x, x, -x, x for the 2D-HN. Quadrature detection in the indirect dimension was achieved through the STATES-TPPI approach incrementing phase ϕ_1 (CON) and ϕ_4 (HN).

The length of the delays was: d_1= 1.7 s; Δ= 16.6 ms; Δ_1 = 4.5 ms; Δ_2= 2.7 ms; ε = ½ duration of adiabatic pulse (250 µs); ε´= t_1(0) + duration of adiabatic pulse (500 µs).

Virtual decoupling of the C′-C^{α} coupling in the 2D-CON was achieved by acquiring for each increment both the IP and AP component of the signals and combining them.

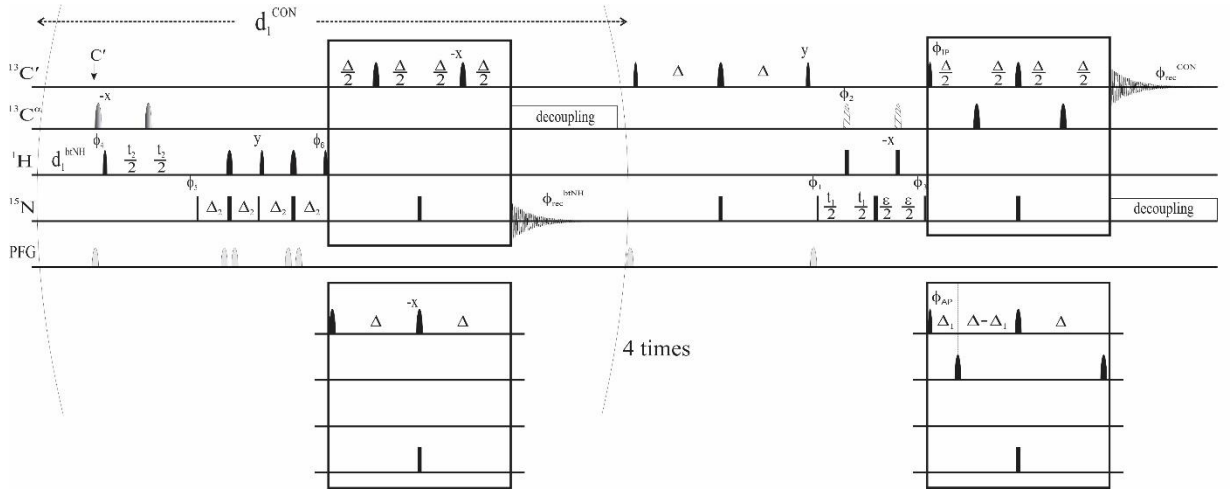

Figure S2. CON//btNH pulse sequence scheme.

Narrow and wide black rectangles represent $\pi/2$ and π non-selective pulses; narrow and wide black symbols represent $\pi/2$ and π band-selective pulses (Q5 and Q3 shapes of 300 and 231 µs respectively), hatched pulses are adiabatic inversion pulse on C′ and C^{α} (smoothed Chirp 500 µs 80 kHz sweep and 20% smooting), the shaded shapes are Bip pulses.

The following phase cycling was employed for the CON//btNH: ϕ_1 = x, -x; ϕ_2 = 2(x), 2(-x); ϕ_3 = 4(x), 4(-x) and ϕ_{rec}^{CON}= x, -x, x, -x, -x, x, -x, x for the 2D-CON and ϕ_4 =y, -y, x, -x; ϕ_5 = y ϕ_6 = x and ϕ_{rec}^{btNH} = x, -x, -y, y for the 2D-btNH. Quadrature detection in the indirect dimension was achieved through the STATES-TPPI approach incrementing phase ϕ_1 for the CON and through the Echo/Antiecho approach by incrementing phase ϕ_4 and ϕ_5.

The length of the delays was: d_1= 2.35 s; Δ= 16.6 ms; Δ_1 = 4.5 ms; Δ_2= 2.7 ms; ε= $t_1(0)$ + duration of adiabatic pulse (500 µs).

Virtual decoupling of the C'-C^{α} coupling in the 2D-CON was achieved by acquiring for each increment both the IP and AP component of the signals. The same approach was also employed to achieve heteronuclear decoupling (C'-N) during acquisition of the ^{15}N FIDs in order to preserve the C' polarization for the subsequent CON experiment. Band selective C^{α} decoupling was achieved using a Q3 pulse in a P5M4 supercycle.

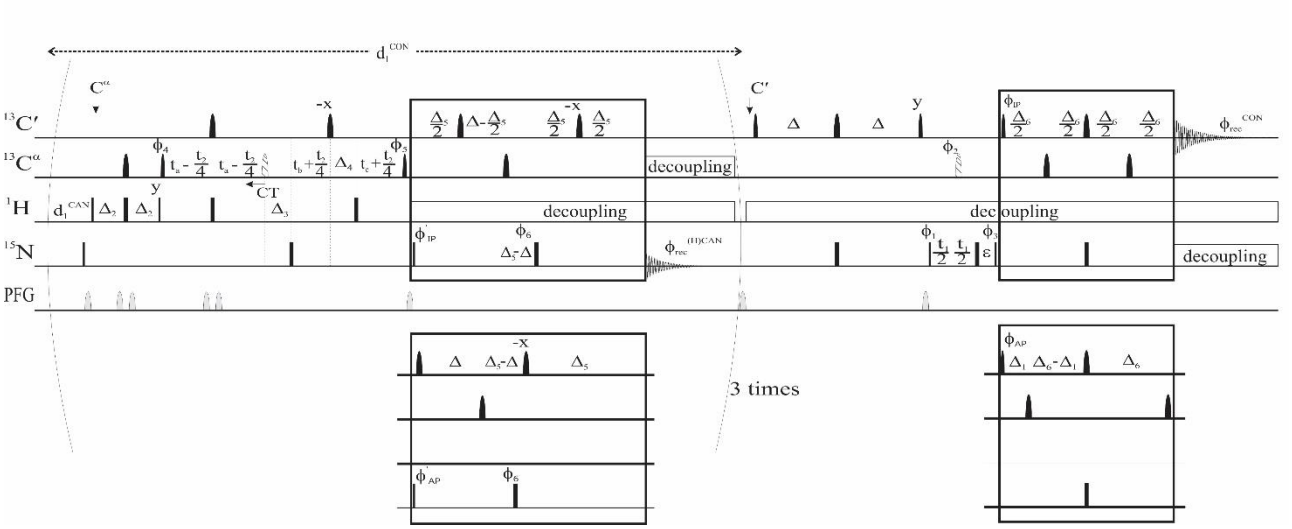

Figure S3. CON//(H)CAN pulse sequence scheme.

Narrow and wide black rectangles represent π/2 and π non-selective pulses; narrow and wide black symbols represent π/2 and π band-selective pulses (Q5 and Q3 shapes of 300 and 231 µs respectively), hatched pulses are adiabatic inversion pulse on C′ and C^{α} (smoothed Chirp 500 µs 80 kHz sweep and 20% smooting).

The following phase cycling was employed for the CON//(H)CAN: ϕ_1 = x, -x; ϕ_2 = 2(x), 2(-x); ϕ_3 = 4(x), 4(-x) ; ϕ^{IP} = x ; ϕ^{AP} = -y and ϕ_{rec}^{CON}= x, -x, x, -x, -x, x, -x, x for the 2D-CON and ϕ_4 = x, –x, ϕ_5 = 4(x), 4(-x) ϕ_6 = 8(x) 8(-x) ; ϕ'^{IP} = 2(x), 2(-x) ; ϕ'^{AP} = 2(y), 2(-y) and $\phi_{rec}^{(H)CAN}$ = x, -x, -x, x, -x, x, x, -x for the 2D-(H)CAN. Quadrature detection in the indirect dimension was achieved through STATES-TPPI approach incrementing phase ϕ_1 (CON) and ϕ_4 ((H)CAN).

The length of the delays was: d_1= 2.5 s; Δ= 12.4 ms; Δ_1 = 4.5 ms; Δ_2= 1.7 ms; Δ_3= 1.9 ms; Δ_4= 1.4 ms; Δ_5= 4.2 ms; Δ_6= 16.6 ms. t_a, t_b and t_c were used to achieve the constant time mode for the $^{13}C^{\alpha}$ indirect dimension.

Virtual decoupling of the C′-C^{α} coupling in the CON was achieved by acquiring for each increment both the IP and AP component of the signals. The same approach was also employed to achieve heteronuclear decoupling (C'-N) during acquisition of the ^{15}N FIDs in order to preserve the C' polarization for the subsequent CON experiment. Band selective C^{α} decoupling was achieved using a Q3 pulse in a P5M4 supercycle.

Pulse sequence CON//HN

```
;ut_con_fhsqchn
;avance-version

;Dataset 1 (F1)
;fhsqcf3gpph
;avance-version (12/01/11)
;2D H-1/X correlation via double inept transfer
;
;      F1(HN) -> F3(N,t1) -> F1(HN,t2)
;
;phase sensitive
;with decoupling during acquisition
;
;(S. Mori, C. Abeygunawardana, M. O'Neil-Johnson & P.C.M. van Zijl,
;   J. Magn. Reson. B 108, 94-98 (1995) )
;
;$CLASS=HighRes
;$DIM=2D
;$TYPE=
;$SUBTYPE=
;$COMMENT=


;Dataset 2 (F2)
;CON
;2D sequence with
;   13C detected correlation for triple resonance using
;      inept transfer steps
;
;      F1(C=O) -> F3(N,t1) -> F1(C=O,t2)
;
;on/off resonance 13C pulses using shaped pulses
;phase sensitive (t1)
;using IPAP scheme for virtual decoupling
;(use parameterset C_CON_IASQ)
;
;W. Bermel, I. Bertini,L. Duma, I.C. Felli, L. Emsley,  R. Pierattelli,
;   P.R. Vasos, Angew. Chem. Int. Ed. 44, 3089-3092 (2005)
;(L. Duma, S. Hediger, A. Lesage & L. Emsley,
;   J. Magn. Reson. 164, 187-195 (2003) )
;
;$CLASS=HighRes
;$DIM=2D
;$TYPE=
;$SUBTYPE=
;$COMMENT=


prosol relations=<triple>


#include <Avance.incl>
#include <Delay.incl>
#include <Grad.incl>


"p2=p1*2"
"p22=p21*2"
"d11=30m"
"d12=20u"
"d26=1s/(cnst4*4)"

"d22=4.5m"
"d23=16.6m"

"in31=inf1/2"
"in32=in2/2"
```

```
"d31=3u"
"d32=3u"


"DELTA=d19-p22/2"
"DELTA1=d26-p16-d16-p27*3-d19*5-p1*2/PI"
"DELTA2=d26-p16-d16-p27*2-p0-d19*5-de-8u"
"DELTA3=d31+larger(p2,p8)/2"
"DELTA4=p21*2/PI"
"DELTA5=d32*2+p8"
"DELTA6=d23/2-p14/2"
"DELTA7=d23-d22-p14"

"TAU=d26-p16-d16-4u"


"l0=1"

"l3=td1/2"


"spoff2=0"
"spoff3=0"
"spoff5=bf2*((cnst22-cnst21)/1000000)"
"spoff8=0"
"spoff13=bf2*((cnst26-cnst21)/1000000)"


1 4u ze1
  4u ze2

2 d11 do:f1 do:f3
  3m
3 12m
4 6m
5 d1

; fhsqc

  20u fq=cnst47(bf ppm):f3
  d12 pl1:f1 pl3:f3
  50u UNBLKGRAD

  (p1 ph11)
  4u
  p16:gp1
  d16
  TAU pl3:f3
  (center (p2 ph11) (p22 ph16):f3 )
  4u
  TAU
  p16:gp1
  d16
  (p1 ph12)

  4u
  p16:gp2
  d16
  (p8:sp13 ph17):f2
  4u

  (p21 ph13):f3
  DELTA3
  (p22 ph13):f3
  DELTA4
  d31

  (center (p2 ph15) (p8:sp13 ph11):f2 )
```

```
  d31
  DELTA4
  (p22 ph14):f3
  DELTA3
  (p21 ph14):f3

  4u
  p16:gp2
  d16

  (p1 ph17)
  p16:gp3
  d16 pl18:f1
  DELTA1
  p27*0.231 ph18
  d19*2
  p27*0.692 ph18
  d19*2
  p27*1.462 ph18
  DELTA
  (p22 ph11):f3
  DELTA
  p27*1.462 ph19
  d19*2
  p27*0.692 ph19
  d19*2
  p0*0.231 ph19
  4u
  p16:gp3
  d16
  4u BLKGRAD
  DELTA2 pl16:f3

  goscnp1 ph31 cpd3:f3


; con

  4u do:f3
  50u UNBLKGRAD

  p16:gp5
  d16

  20u pl19:f1 pl3:f3
  20u fq=cnst21(bf ppm):f2
  20u fq=cnst57(bf ppm):f3
  d12 cpds1:f1

  (p13:sp2 ph1):f2
  d23
  (center (p14:sp3 ph1):f2 (p22 ph1):f3 )
  d23
  (p13:sp8 ph2):f2

  p16:gp4
  d16

  (p21 ph3):f3
  d32
  (p8:sp13 ph5):f2
  d32
  (p22 ph1):f3
  DELTA5
  (p21 ph4):f3

  if "l0 %2 == 1"
     {
     (p13:sp2 ph1):f2
     DELTA6
```

```
      (p14:sp5 ph1):f2
      DELTA6
      (center (p14:sp3 ph1):f2 (p22 ph1):f3 )
      DELTA6
      (p14:sp5 ph1):f2
      DELTA6 pl16:f3
      }
   else
      {
      (p13:sp2 ph6):f2
      d22
      (p14:sp5 ph1):f2
      DELTA7
      (center (p14:sp3 ph1):f2 (p22 ph1):f3 )
      DELTA6
      DELTA6 pl16:f3
      (p14:sp5 ph1):f2
      }

   4u BLKGRAD
   go2=2 ph30 cpd3:f3

   d11 do:f1 do:f3 wr2 #1 if2 #1 zd2

;exp_f2 ipap
   3m iu0
   lo to 3 times 2

   3m wr1 #0 if1 #0 zd1

;exp_f1 phase
   3m ip13
   3m ip16
;exp_f2 phase
   3m ip3
   lo to 4 times 2

;exp_f1 delay
   3m id31
;exp_f2 delay
   3m id32
   lo to 5 times l3

exit


ph1=0
ph2=1
ph3=0 2
ph4=0 0 0 0 2 2 2 2
ph5=0 0 2 2
ph6=3

ph11=0
ph12=1
ph13=0 2
ph14=0 0 0 0 2 2 2 2
ph15=0 0 2 2
ph16=0
ph17=2
ph18=1
ph19=3

ph30=0 2 0 2 2 0 2 0
ph31=0 2 0 2 2 0 2 0

;pl1 : f1 channel - power level for pulse (default)
;pl3 : f3 channel - power level for pulse (default)
;pl16: f3 channel - power level for CPD/BB decoupling
;pl18: f1 channel - power level for 3-9-19-pulse (watergate)
```

```
;pl19: f1 channel - power level for CPD/BB decoupling
;sp2 : f1 channel - shaped pulse  90 degree  (on resonance)
;sp3 : f1 channel - shaped pulse 180 degree  (on resonance)
;sp5 : f1 channel - shaped pulse 180 degree  (Ca off resonance)
;sp8 : f1 channel - shaped pulse  90 degree  (on resonance)
;                  for time reversed pulse
;sp13: f1 channel - shaped pulse 180 degree  (adiabatic)
;p0 : f1 channel -  90 degree pulse at pl18
;                   use for fine adjustment
;p1 : f1 channel -  90 degree high power pulse
;p2 : f1 channel - 180 degree high power pulse
;p8 : f1 channel - 180 degree shaped pulse for inversion (adiabatic)
;p13: f1 channel -  90 degree shaped pulse
;p14: f1 channel - 180 degree shaped pulse
;p16: homospoil/gradient pulse                          [1 msec]
;p21: f3 channel -  90 degree high power pulse
;p22: f3 channel - 180 degree high power pulse
;p27: f1 channel -  90 degree pulse at pl18
;d1 : relaxation delay; 1-5 * T1
;d11: delay for disk I/O                                [30 msec]
;d12: delay for power switching                         [20 usec]
;d16: delay for homospoil/gradient recovery
;d19: delay for binomial water suppression
;d22: 1/(4J(COCa))                                      [4.5 msec]
;d23: 1/(4J(NCO))                                       [16.6 msec]
;d26: 1/(4J(NH))
;d31: incremented delay (2D, exp 1)                     [3 usec]
;d32: incremented delay (2D, exp 2)                     [3 usec]
;cnst4: = J(NH)
;cnst21: CO chemical shift (offset, in ppm)
;cnst22: Calpha chemical shift (offset, in ppm)
;cnst26: Call chemical shift (offset, in ppm)           [101 ppm]
;cnst47: N(H) chemical shift (offset, in ppm)
;cnst57: N chemical shift (offset, in ppm)
;o1p: CO chemical shift (cnst21)
;l0: flag to switch between inphase and antiphase
;l3 : loop for 2D experiment = td1/2
;inf1: 1/SW(N) = 2 * DW(N)
;in2 : 1/SW(N) = 2 * DW(N) (inf1 of exp 2, N all)
;in31: 1/(2 * SW(N)) =  DW(N)
;nd31: 2
;in32: 1/(2 * SW(N)) =  DW(N)
;nd32: 2
;ns: 8 * n
;ds: >= 32
;td1: number of experiments in F1
;       (number of experiments after IPAP processing)
;FnMODE: States-TPPI (or TPPI) in F1
;cpds1: decoupling according to sequence defined by cpdprg1
;cpd3: decoupling according to sequence defined by cpdprg3
;pcpd1: f1 channel - 90 degree pulse for decoupling sequence
;pcpd3: f3 channel - 90 degree pulse for decoupling sequence

;for z-only gradients:
;gpz1: 50%
;gpz2: 80%
;gpz3: 31%
;gpz4: 19%
;gpz5: 60%

;use gradient files:
;gpnam1: SMSQ10.100
;gpnam2: SMSQ10.100
;gpnam3: SMSQ10.100
;gpnam4: SMSQ10.100
;gpnam5: SMSQ10.100

;use AU-program splitcomb [ipap 2] to process data

;$Id: $
```

Pulse sequence CON//btNH

```
;ut_con_n_btnh
;avance-version

;Dataset 1 (F1)
;c_con_iasq
;avance-version
;CON
;2D sequence with
;   13C detected correlation for triple resonance using
;      inept transfer steps
;
;      F1(C=O) -> F3(N,t1) -> F1(C=O,t2)
;
;on/off resonance 13C pulses using shaped pulses
;phase sensitive (t1)
;using IPAP scheme for virtual decoupling
;(use parameterset C_CON_IASQ)
;
;W. Bermel, I. Bertini,L. Duma, I.C. Felli, L. Emsley,  R. Pierattelli,
;   P.R. Vasos, Angew. Chem. Int. Ed. 44, 3089-3092 (2005)
;(L. Duma, S. Hediger, A. Lesage & L. Emsley,
;   J. Magn. Reson. 164, 187-195 (2003) )
;
;
;Dataset 2 (F2)
;dummy dataset
;
;
;Dataset 3 (F3)
;nb_hntrosy_f2ig
;avance-version (17/02/10)
;2D 15N shift correlation
;
;      F2(HN,t1) -> F3(N,t2)
;
;with refocussing of chemical shifts
;phase sensitive
;using semi-constant time in t1
;(use parameterset )
;
;(R. Schnieders, C. Richter, S. Warhaut, V. de Jesus, S. Keyhani,
;   E. Duchardt-Ferner, H. Keller, J. WÃ¶hnert, L.T. Kuhn, A.L. Breeze,
;   W. Bermel, H. Schwalbe & B. FÃ¼rtig, ;   J. Biomol. NMR 69, 31â€“44 (2017) )
;(K. Takeuchi, H. Arthanari, I. Shimada & G. Wagner, J. Biomol. NMR 63, 1â€“9 (2015) )
;(K. Takeuchi, H. Arthanari, M. Imai & G. Wagner, J. Biomol. NMR 64, 143â€“151 (2016) )
;
;$CLASS=HighRes
;$DIM=2D
;$TYPE=
;$SUBTYPE=
;$COMMENT=


prosol relations=<triple_c>


#include <Avance.incl>
#include <Delay.incl>
#include <Grad.incl>


"p22=p21*2"
"d11=30m"
"d12=20u"
"d26=1s/(cnst4*4)"

"d22=4.5m"
```

```
"d23=16.6m"


"p42=(bwfac42/(cnst55*cnst52*bf2))*1000000"
"spw42=plw2/((p42*90.0)/(p3*totrot42))*((p42*90.0)/(p3*totrot42))*(integfac42*integ-
fac42)"
"spoal42=0.5"
"spoff42=bf2*(cnst54/1000000)-o2"

"p43=(bwfac43/(cnst55*cnst53*bf2))*1000000"
"spw43=plw2/((p43*90.0)/(p3*totrot43))*((p43*90.0)/(p3*totrot43))*(integfac43*integ-
fac43)"
"spw44=plw2/((p43*90.0)/(p3*totrot44))*((p43*90.0)/(p3*totrot44))*(integfac44*integ-
fac44)"
"spoal43=0"
"spoal44=1"
"spoff43=bf2*(cnst54/1000000)-o2"
"spoff44=bf2*(cnst54/1000000)-o2"


"in31=inf1/2"
"in32=in2/2"

"d31=3u"
"d32=in32/2-p39/2"


"d60=d1-(d61+d59)*4-d58"


"DELTA=d31"
"DELTA1=d23/2-p12/2"
"DELTA2=d23-d22-p12"
"DELTA11=d26-larger(p22,p42)/2-p16-d16"
"DELTA12=d26-larger(p22,p42)/2-p16-d16-p21*2/PI"
"DELTA13=d26-larger(p22,p42)/2-p16-d16-de"
"DELTA14=d23/2-p12/2"


"l0=0"
"l3=l22/2"
"l10=1"
"l13=td1/(8*l22)"
"l30=0"


"spoff4=bf1*((cnst26-cnst22)/1000000)"
"spoff13=bf1*((cnst26-cnst21)/1000000)"
"spoff23=0"
"spoff24=0"
"spoff25=0"
"spoff26=bf1*((cnst22-cnst21)/1000000)"
"spoff27=bf1*((cnst21-cnst22)/1000000)"


1 4u ze1
  4u ze3
2 d11 do:f3
  3m
3 3m
4 3m
5 6m
6 9m
7 12.02m
8 3m

  d60
  50u UNBLKGRAD

goscnp2 ph31
```

```
  p16:gp2
  d16

;n_trhn

  d12 pl19:f1 pl3:f3
  20u fq=cnst22(bf ppm):f1

  "cnst31=(l30%2)*90"

  3m ip18+cnst31

11 d61

  (p39:sp4 ph17):f1

  if "l0 %2 == 1"
     {
     (p43:sp44 ph13+ph18):f2
     }
  else
     {
     (p43:sp44 ph14+ph18):f2
     }
  d32
  (p39:sp4 ph1+ph18):f1
  d32

  (p21 ph15+ph18):f3
  DELTA11
  p16:gp3
  d16
  4u
  (center (p42:sp42 ph1+ph18):f2 (p22 ph1+ph18):f3 )
  4u
  p16:gp3
  d16
  DELTA11
  (p21 ph1+ph18):f3

  (p43:sp43 ph2+ph18):f2
  DELTA12
  p16:gp4
  d16
  4u
  (center (p42:sp42 ph1+ph18):f2 (p22 ph1+ph18):f3 )
  4u
  p16:gp4
  d16
  DELTA13
  4u BLKGRAD
  (p43:sp44 ph16+ph18):f2

  if "l30 %2 == 0"
     {
     DELTA14
     (p12:sp27 ph1):f1
     DELTA14
     (p22 ph1):f3
     DELTA14
     (p12:sp27 ph17):f1
     DELTA14 pl19:f1
     }
  else
     {
     (p12:sp27 ph1):f1
     DELTA14
     DELTA14
     (p22 ph1):f3
```

```
      (p12:sp27 ph17):f1
      DELTA14
      DELTA14 pl19:f1
      }

  goscnp3 ph30 cpd1:f1

  4u do:f1
  lo to 11 times 4

  50u UNBLKGRAD

  p16:gp5
  d16

;con

  20u pl3:f3
  20u fq=cnst21(bf ppm):f1

  (p11:sp23 ph1)
  d23
  (center (p12:sp24 ph1) (p22 ph1):f3 )
  d23
  (p11:sp25 ph2)

  p16:gp1
  d16

  (p21 ph3):f3
  d31
  (center (p8:sp13 ph5):f1 (p44:sp3 ph1):f2 )
  d31
  (p22 ph1):f3
  DELTA
  (center (p8:sp13 ph1):f1 (p44:sp3 ph7):f2 )
  DELTA
  (p21 ph4):f3

  if "l10 %2 == 1"
     {
     (p11:sp23 ph1)
     DELTA1
     (p12:sp26 ph1)
     DELTA1
     (center (p12:sp24 ph1) (p22 ph1):f3 )
     DELTA1
     (p12:sp26 ph1)
     DELTA1 pl16:f3
     }
  else
     {
     (p11:sp23 ph6)
     d22
     (p12:sp26 ph1)
     DELTA2
     (center (p12:sp24 ph1) (p22 ph1):f3 )
     DELTA1
     DELTA1 pl16:f3
     (p12:sp26 ph1)
     }

  4u BLKGRAD

  go1=2 ph31 cpd3:f3

  d11 do:f3 wr1 #0 if1 #0 zd1
  3m wr2 #1 if2 #1 zd2

;exp_f1 ipap
```

```
  3m iu10
  lo to 3 times 2

;exp_f1 phase
  3m ip3
  lo to 4 times 2

;exp_f1 delay
  3m id31
  lo to 5 times l13

  3m wr3 #2 if3 #2 zd3

  3m iu30
  lo to 6 times 2

;exp_f2 phase
  3m ip15*2
  3m ip16*2
  3m iu0
  lo to 7 times 2

;exp_f2 delay
  3m id32
  3m
  20u
  3m
  3m
  lo to 8 times l3


exit


ph1=0
ph2=1
ph3=0 2
ph4=0 0 0 0 2 2 2 2
ph5=0 0 2 2
ph6=3
ph7=2
ph13=1 3 0 2
ph14=3 1 0 2
ph15=1
ph16=0
ph17=2
ph18=0
ph30=0 2 3 1
ph31=0 2 0 2 2 0 2 0


;pl1 : f1 channel - power level for pulse (default)
;pl3 : f3 channel - power level for pulse (default)
;pl16: f3 channel - power level for CPD/BB decoupling
;pl19: f1 channel - power level for CPD/BB decoupling
;sp3 : f2 channel - shaped pulse 180 degree (Bip720,50,20.1)
;sp4 : f1 channel - shaped pulse 180 degree (Bip720,100,10.1)
;sp13: f1 channel - shaped pulse 180 degree  (adiabatic)
;sp23: f1 channel - shaped pulse  90 degree  (on resonance)
;sp24: f1 channel - shaped pulse 180 degree  (on resonance)
;sp25: f1 channel - shaped pulse  90 degree  (on resonance)
;                   for time reversed pulse
;sp26: f1 channel - shaped pulse 180 degree  (Ca off resonance)
;sp27: f1 channel - shaped pulse 180 degree  (C=O off resonance)
;sp42: f2 channel - shaped pulse 180 degree (Reburp.1000)
;sp43: f2 channel - shaped pulse  90 degree (Eburp2.1000)
;sp44: f2 channel - shaped pulse  90 degree (Eburp2tr.1000)
;p8 : f1 channel - 180 degree shaped pulse for inversion (adiabatic)
;p11: f1 channel -  90 degree shaped pulse
;p12: f1 channel - 180 degree shaped pulse
```

```
;p16: homospoil/gradient pulse                          [1 msec]
;p21: f3 channel -  90 degree high power pulse
;p22: f3 channel - 180 degree high power pulse
;p39: f1 channel - 180 degree shaped pulse for refocussing
;                     Bip720,100,10.1 (160us at 600.13 MHz)
;p42: f2 channel - 180 degree shaped pulse for refocussing
;                     Reburp.1000               (1.4ms at 600.13 MHz)
;p43: f2 channel -  90 degree shaped pulse for excitation
;                     Eburp2.1000/Eburp2tr.1000 (1.7ms at 600.13 MHz)
;p44: f2 channel - 180 degree shaped pulse for refocussing
;                     Bip720,50,20.1            (200us at 600.13 MHz)
;d1 : relaxation delay; 1-5 * T1
;d11: delay for disk I/O                                [30 msec]
;d12: delay for power switching                         [20 usec]
;d16: delay for homospoil/gradient recovery
;d22: 1/(4J(COCa))                                      [4.5 msec]
;d23: 1/(4J(NCO))                                       [16.6 msec]
;d26: 1/(4J)NH
;d31: incremented delay (2D, exp 1))                    [3 usec]
;d32: incremented delay (2D, exp 3)): in32/2-p39/2
;d58: = AQ of exp 2 (1H)
;d59: = AQ of exp 3 (15N)
;d60: relaxation delay as executed
;d61: relaxation delay of exp 3
;cnst4: = J(NH)
;cnst21: CO chemical shift (offset, in ppm)
;cnst22: Calpha chemical shift (offset, in ppm)
;cnst26: Call chemical shift (offset, in ppm)          [101 ppm]
;cnst43: compensation of chemical shift evolution during p43
;           Eburp2.1000: 0.69
;cnst52: scaling factor for p42 to compensate for transition region
;           Reburp.1000: 1.426
;cnst53: scaling factor for p43 to compensate for transition region
;           Eburp2.1000: 1.000
;cnst54: H(N) chemical shift (offset, in ppm)
;cnst55: H(N) bandwidth (in ppm)
;o1p: CO chemical shift (cnst21)
;l0 : flag to switch between odd and even increments (exp 3)
;l3 : loop for 2D exp 1 = l22/2
;l13: loop for 2D exp 3 = td1/(8*l22)
;l10: flag to switch between inphase and antiphase (exp 1)
;l22: number of experiments in F1 for exp 3 (after IPAP processing)
;l30: flag to switch between inphase and antiphase (exp 3)
;inf1: 1/SW(N) = 2 * DW(N)
;in2 : 1/SW(H) = 2 * DW(H) (inf1 of exp 3)
;in31: 1/(2 * SW(N)) =  DW(N)
;nd31: 2
;in32: 1/(2 * SW(H)) = DW(H)
;nd32: 2
;ns: 8 * n
;ds: >= 32
;td1: number of experiments in F1
;       (number of experiments after IPAP processing)
;FnMODE: States-TPPI (or TPPI) in F1
;cpd1: decoupling according to sequence defined by cpdprg1: p5m4sp180
;cpd3: decoupling according to sequence defined by cpdprg3
;pcpd1: f1 channel - 180 degree pulse for decoupling sequence
;pcpd3: f3 channel - 90 degree pulse for decoupling sequence
;cpdprg1: p5m4sp180


;for z-only gradients:
;gpz1: 50%
;gpz2: 70%
;gpz3: 31%
;gpz4: 19%
;gpz5: 45%

;use gradient files:
;gpnam1: SMSQ10.100
```

```
;gpnam2: SMSQ10.100
;gpnam3: SMSQ10.100
;gpnam4: SMSQ10.100
;gpnam5: SMSQ10.100


;use AU-program splitcomb [ipap 2] to process data

;Processing (exp 3)

;PHC0(F1): 90
;PHC1(F1): -180
;FCOR(F1): 1


;$Id: $
```

Pulse sequence CON//(H)CAN

```
;ut_con_n_(h)can
;avance-version

;Dataset 1 (F1)
;n_hcan.2
;avance-version
;2D sequence with
;   15N detected correlation for triple resonance using
;      inept transfer steps
;
;      F3(Ha) -> F2(Ca,t1) -> F1(N,t2)
;
;on/off resonance 13C pulses using shaped pulses
;phase sensitive (t1)
;using constant time in t1
;(use parameterset )
;
;M. Gal, K. A. Edmonds, A. G. Milbradt, K. Takeuchi & G. Wagner,
;   J Biomol NMR 51, 497-504 (2011)
;(K. Takeuchi, G. Heffron, Z.-Y. J. Sun, D. P. Frueh & G. Wagner,
;   J Biomol NMR 47, 271-282 (2010))
;
;$CLASS=HighRes
;$DIM=2D
;$TYPE=
;$SUBTYPE=
;$COMMENT=


;Dataset 2 (F2)
;c_con_iasq
;avance-version
;CON
;2D sequence with
;   13C detected correlation for triple resonance using
;      inept transfer steps
;
;      F2(C=O) -> F1(N,t1) -> F2(C=O,t2)
;
;on/off resonance 13C pulses using shaped pulses
;phase sensitive (t1)
;using IPAP scheme for virtual decoupling
;(use parameterset )
;
;W. Bermel, I. Bertini,L. Duma, I.C. Felli, L. Emsley,  R. Pierattelli,
;   P.R. Vasos, Angew. Chem. Int. Ed. 44, 3089-3092 (2005)
;(L. Duma, S. Hediger, A. Lesage & L. Emsley,
;   J. Magn. Reson. 164, 187-195 (2003) )
;
;$CLASS=HighRes
;$DIM=2D
;$TYPE=
;$SUBTYPE=
;$COMMENT=


prosol relations=<triple>


#include <Avance.incl>
#include <Delay.incl>
#include <Grad.incl>


"p2=p1*2"
"p22=p21*2"
"d3=1s/(cnst2*cnst12)"
```

```
"d4=1s/(cnst2*4)"
"d11=30m"
"d12=20u"

"d22=4.5m"
"d23=12.4m"
"d25=16.6m"
"d27=14.3m"


"d32=3u"
"d31=d27/2-d3-p22/2"
"d41=d27/2-larger(p14,p22)/2"
"d51=d23-d27/2-p14/2-p2/2"


"in31=inf1/4"
"in32=in2/2"

"in41=in32"
"in51=in32"

"td1=tdmax(td1,d41*2,in42)"


"d1=(d60+d58)*3 +d59+50m"


"DELTA1=d27-d23-p2/2"
"DELTA2=d3-p14/2-p22/2"
"DELTA3=d25/2"
"DELTA4=d23-d25/2-p14"
"DELTA5=d25-d23"
"DELTA6=d25/2-d12+p1*2/PI-de-4u"
"DELTA7=d32*2+p8"
"DELTA8=d23/2-p14/2"
"DELTA9=d23-d22-p14"


"spoff2=0"
"spoff3=0"
"spoff5=bf2*((cnst21-cnst22)/1000000)"
"spoff7=bf2*((cnst22-cnst21)/1000000)"
"spoff8=0"
"spoff13=bf2*((cnst26-cnst21)/1000000)"
"spoff23=bf2*((cnst23-cnst22)/1000000)"

"l0=0"
"l10=0"

"l3=td1/4"


"acqt0=0"
baseopt_echo


1 4u ze1
  4u ze2
  d1

2 d11 do:f1 do:f3
  3m
3 3m
4 9m
5 3m
6 9m
7 3m

;n_hcan
```

```
8 d11 do:f2 do:f3
  d60

  50u UNBLKGRAD
  4u pl1:f1 pl3:f3

  (p1 ph1):f1
  p16:gp1
  d16 fq=cnst22(bf ppm):f2

  (p21 ph1):f3
  d4
  (center (p14:sp3 ph1):f2 (p22 ph1):f3 )
  d4
  (p21 ph2):f3

  (p13:sp2 ph3):f2
  d41
  (center (p14:sp5 ph1):f2 (p22 ph1):f3 )
  d41
  (p14:sp23 ph1):f2
  DELTA1
  (p2 ph1):f1
  d51
  (p14:sp5 ph10):f2
  DELTA2
  (p22 ph1):f3
  d31
  (p13:sp8 ph4):f2

  4u
  p16:gp2
  d16 pl16:f3
  20u cpd3:f3

  if "l0 %2 == 0"
     {
     (p1 ph5):f1
     DELTA3
     (p14:sp5 ph1):f2
     DELTA4
     (p14:sp3 ph1):f2
     DELTA5
     (p2 ph6):f1
     DELTA3
     (p14:sp5 ph10):f2
     }
  else
     {
     (p1 ph7):f1
     (p14:sp5 ph1):f2
     DELTA3
     DELTA4
     (p14:sp3 ph1):f2
     DELTA5
     (p2 ph6):f1
     (p14:sp5 ph10):f2
     DELTA3
     }

  DELTA6
  d12 pl28:f2
  4u BLKGRAD

  goscnp1 ph31 cpd2:f2
  lo to 8 times 3


;c_con
```

```
  4u do:f2 do:f3
  50m
  50u UNBLKGRAD

  p16:gp3
  d16 fq=cnst21(bf ppm):f2

  4u pl1:f1 pl16:f3
  4u cpd3:f3

  (p13:sp2 ph1):f2
  d23
  (center (p2 ph1):f1 (p14:sp3 ph1):f2 )
  d23
  (p13:sp8 ph2):f2

  p16:gp4
  d16

  (p1 ph13):f1
  d32
  (p8:sp13 ph15):f2
  d32
  (p2 ph1):f1
  DELTA7
  (p1 ph14):f1

  if "l10 %2 == 0"
     {
     (p13:sp2 ph1):f2
     DELTA8
     (p14:sp7 ph1):f2
     DELTA8
     (center (p2 ph1):f1 (p14:sp3 ph1):f2 )
     DELTA8
     (p14:sp7 ph1):f2
     DELTA8 pl19:f1
     }
  else
     {
     (p13:sp2 ph16):f2
     d22
     (p14:sp7 ph1):f2
     DELTA9
     (center (p2 ph1):f1 (p14:sp3 ph1):f2 )
     DELTA8
     DELTA8 pl19:f1
     (p14:sp7 ph1):f2
     }

  4u BLKGRAD

  go2=2 ph30 cpd1:f1

  d11 do:f1 do:f3 wr2 #1 if2 #1 zd2

;exp_f2 ipap
  3m iu10
  lo to 3 times 2

;exp_f2 phase
  3m dp13
  lo to 4 times 2

  3m wr1 #0 if1 #0 zd1

;exp_f1 ipap
  3m iu0
```

```
;exp_f2 delay
  3m id32
  lo to 5 times 2

;exp_f1 phase
  3m ip3
  lo to 6 times 2

;exp_f1 delay
  3m id31
  3m dd41
  3m id51

  lo to 7 times l3

exit


ph1=0
ph2=1
ph3=0 2
ph4=0 0 0 0 2 2 2 2
ph5=0 0 2 2
ph6=0 0 0 0 0 0 0 0 2 2 2 2 2 2 2 2
ph7=1 1 3 3
ph10=2

ph13=0 2
ph14=0 0 0 0 2 2 2 2
ph15=0 0 2 2
ph16=3

ph29=0
ph30=0 2 0 2 2 0 2 0
ph31=0 2 2 0 2 0 0 2


;pl1 : f1 channel - power level for pulse (default)
;pl2 : f2 channel - power level for pulse (default)
;pl3 : f3 channel - power level for pulse (default)
;pl16: f3 channel - power level for CPD/BB decoupling
;pl19: f1 channel - power level for CPD/BB decoupling
;pl28: f2 channel - power level for CPD/BB decoupling
;sp2: f2 channel - shaped pulse  90 degree  (on resonance)
;sp3: f2 channel - shaped pulse 180 degree  (on resonance)
;sp5: f2 channel - shaped pulse 180 degree  (C=O off resonance)
;sp7: f2 channel - shaped pulse 180 degree  (Ca off resonance)
;sp8: f2 channel - shaped pulse  90 degree  (on resonance)
;                    for time reversed pulse
;sp13: f2 channel - shaped pulse 180 degree  (adiabatic)
;sp23: f2 channel - shaped pulse 180 degree  (Cali off resonance)
;p1 : f1 channel -  90 degree high power pulse
;p2 : f1 channel - 180 degree high power pulse
;p8 : f2 channel - 180 degree shaped pulse for inversion (adiabatic)
;p13: f2 channel -  90 degree shaped pulse
;p14: f2 channel - 180 degree shaped pulse
;p16: homospoil/gradient pulse                          [1 msec]
;p21: f3 channel -  90 degree high power pulse
;p22: f3 channel - 180 degree high power pulse
;d1 : relaxation delay as executed; 1-5 * T1
;d3 : 1/(n*J(CH)), n = cnst12
;d4 : 1/(4J(CH))
;d11: delay for disk I/O                                [30 msec]
;d12: delay for power switching                         [20 usec]
;d16: delay for homospoil/gradient recovery
;d22: 1/(4J(COCa))                                      [4.5 msec]
;d23: 1/(4J(NCO))                                       [12.4 msec]
;d25: 1/(4J'(NCO))                                      [16.6 msec]
;d27: 1/(2J(CaCb))                                      [14.3 msec]
;d31 : incremented delay (2D, exp 1) = d27/2-d3-p22/2
```

```
;d32 : incremented delay (2D, exp 2)             [3 usec]
;d41: decremented delay (2D, exp 1) = d27/2-larger(p14,p22)/2
;d51: incremented delay (2D) = d23-d27/2-p14/2-p2/2
;d58: = AQ of exp 1 (15N)
;d59: = AQ of exp 2 (13C)
;d60: relaxation delay for exp 1
;cnst2: = J(CH)                                          [145 Hz]
;cnst12: for multiplicity selection = 4 for all but Gly, 5 including Gly
;cnst21: CO chemical shift (offset, in ppm)
;cnst22: Calpha chemical shift (offset, in ppm)
;cnst23: Caliphatic chemical shift (offset, in ppm)
;cnst26: Call chemical shift (offset, in ppm)          [101 ppm]
;o1p: CO chemical shift (cnst21)
;l0 : flag to switch between inphase and antiphase (exp 1)
;l3 : loop for 2D experiment = td1/4
;l10: flag to switch between inphase and antiphase (exp 2)
;inf1: 1/SW(Ca) = 2 * DW(Ca)
;in2 : 1/SW(N) = 2 * DW(N) (inf1 of exp 2)
;in31: 1/(4 * SW(Ca)) = (1/2) DW(Ca)
;nd31: 4
;in32: 1/(2 * SW(N)) = DW(N)
;nd32: 2
;in42: = in32
;in52: = in32
;ns: 4 * n
;ds: >= 32
;td1: number of experiments in F1
;       (number of experiments after IPAP processing)
;FnMODE: States-TPPI (or TPPI) in F1
;cpd1: decoupling according to sequence defined by cpdprg1
;cpd2: decoupling according to sequence defined by cpdprg2: p5m4sp180
;cpd3: decoupling according to sequence defined by cpdprg3
;pcpd1: f1 channel - 90 degree pulse for decoupling sequence
;pcpd2: f2 channel - 180 degree pulse for decoupling sequence
;pcpd3: f3 channel - 90 degree pulse for decoupling sequence

;for z-only gradients:
;gpz1: 50%
;gpz2: 40%
;gpz3: 60%
;gpz4: 30%

;use gradient files:
;gpnam1: SMSQ10.100
;gpnam2: SMSQ10.100
;gpnam3: SMSQ10.100
;gpnam4: SMSQ10.100

;use AU-program splitcomb [ipap 2] to process data

;$Id: $
```